CCS Chemistry

MINI REVIEW

Received: Dec. 3, 2024 | Accepted: Dec. 31, 2024 | Published: Jan. 29, 2025

Chemical Synthesis Driven by High Pressure

Wenya Zhao[1†], Jie Zhang[2†], Zhongxiong Sun[3†], Guanjun Xiao[1*], Haiyan Zheng[2], Kuo Li[2*], Man-Rong Li[4*] & Bo Zou[1*]

[1]State Key Laboratory of High Pressure and Superhard Materials, College of Physics, Jilin University, Changchun 130012, [2]Center for High Pressure Science & Technology Advanced Research, Beijing 100193, [3]Key Laboratory of Bioinorganic and Synthetic Chemistry of Ministry of Education, School of Chemistry, Sun Yat-sen University, Guangzhou 510275, [4]School of Chemistry and Chemical Engineering, Hainan University, Haikou 570228

**Corresponding authors: xguanjun@jlu.edu.cn; likuo@hpstar.ac.cn; limanrong@hainanu.edu.cn; zoubo@jlu.edu.cn;*
[†]W. Zhao, J. Zhang, and Z. Sun contributed equally to this work.

Cite this: *CCS Chem.* **2025**, 7, 1250–1271
DOI: 10.31635/ccschem.024.202405293

The chemical synthesis of functional materials is inseparable from national defense, medical treatment, national economy, and people's livelihood. Traditional organic and inorganic materials are approaching their performance limit. Therefore, the design and exploitation of novel functional materials are imminent and of significance for sustainable development. This review outlines the current progress and future prospects of chemical synthesis driven by high pressure, including organic and inorganic synthesis, as well as high-pressure phase retention. Based on the latest works, the basic mechanism of high-pressure chemical synthesis and three potential strategies for high-pressure phase harvesting are revealed. Finally, the challenge and outlook of high-pressure-guided chemical synthesis are summarized. We sincerely hope that this review will provide guidance for designing high-performance materials by expanding the paths of chemical synthesis, thus greatly exploiting the existing materials world with newly emerging and enhanced functionalities.

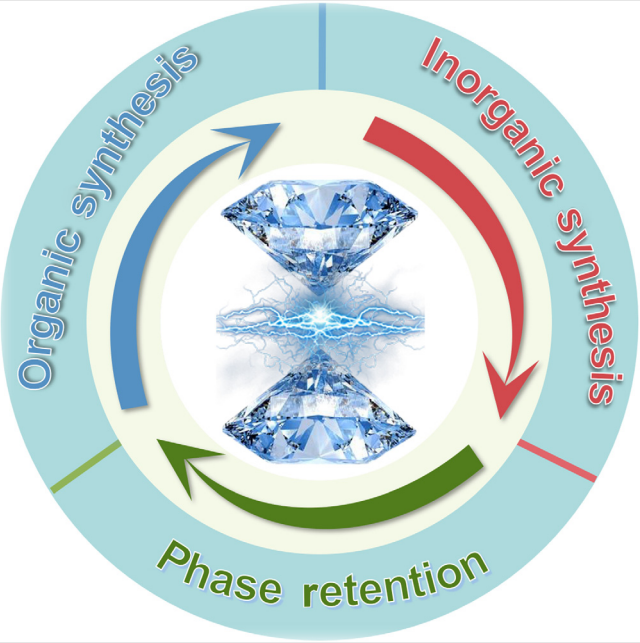

Keywords: **high pressure, chemical synthesis, organic synthesis, inorganic synthesis, phase retention**

Introduction

The chemical synthesis of new functional materials is of great significance for national defense, medical treatment, national economy, and people's livelihood.[1,2] Designing advanced materials based on organic and inorganic chemistry has promoted innovation and development in a range of scientific and technological fields. Organic materials (e.g., polymers and plastics) and inorganic materials (e.g., ceramics and glass) are ubiquitous in all corners and aspects of our daily lives. Now we are in the middle of a scientific revolution in the environment, energy, sustainability, and information technology sectors. So far, the revolution has relied on traditional materials, such as silicon for photovoltaic power generation, as well as graphite and oxide for lithium-ion batteries.[3]

DOI: 10.31635/ccschem.024.202405293
Citation: *CCS Chem.* **2025**, 7, 1250–1271
Link to VoR: https://doi.org/10.31635/ccschem.024.202405293

However, these conventional materials are approaching their performance limits. Therefore, developing new functional materials is necessary in order to adapt to emerging applications in a sustainable way.

Strategies for the development of new materials and properties include intrinsic structural design induced by chemical pressure and extrinsic stimulus under different environmental conditions. The generation of internal chemical pressure usually requires changes to the original chemical composition. For example, the internal chemical pressure occurred by replacing Sn with Sb, Ge, and Cd with smaller atomic radii causes lattice shrinkage, thereby increasing the energy of the Σ-band.[4] In addition, solution blending is used to form ordered branched polyethyleneimine-one-dimensional lepidocrocite hybrids to prevent one-dimensional to two-dimensional structural evolution.[5] Likewise, external stimuli are able to effectively avoid the influence of complex chemical composition changes, thus providing comparably convenient methods for the structural design and functional regulation. Pressure, as one of the thermodynamic variables and stimulus, has been used as a controllable parameter to drive a given substance across multiple phases and to establish the phase diagram of a condensed matter system. The application of high pressure provides an additional dimension to chemical phase space, opening up an unexplored expanse bearing tremendous potential for discoveries. Pressure can fundamentally shorten the distance between molecules or atoms, thereby changing the periodicity of structure and yielding more new materials than ever before.[6–8] High-pressure synthesis methods possess unlimited potential in different research fields.

This review will introduce the latest developments in high-pressure chemical synthesis and the retention of high-pressure phase. In the high-pressure chemical synthesis section, we will summarize some of the organic and inorganic high-performance materials synthesized under high pressure and discuss their underlying synthetic mechanisms. As for the high-pressure phase retention, we will excavate materials with better performance from possible stabilized mechanisms of high-pressure metastable phases, such as the nano-size effect, steric hindrance effect, and hydrogen bonding cooperativity effect. Overall, we have mainly focused on quenching the exotic structures or superior properties at high pressure to the ambient conditions through the strategy of chemical synthesis driven by high pressure. There are three types of channels for obtaining new functional materials regarding harvesting high-pressure phases through high-pressure treatment. Firstly, chemical reaction between multiple organic components in a small diamond anvil cell under high pressure; secondly, chemical reactions between multiple inorganic components in a large volume press under high pressure; and thirdly, metastable phase retention of single component at high pressure after structural phase transition. Last, we intend to summarize the potential research directions of high-pressure synthesis, and look into the future development of the retention of the high-pressure phase.

High-Pressure Organic Synthesis

High pressure can significantly regulate the stacking of organic molecules and the intermolecular distances, promote phase changes and chemical bond reconstruction, and provide new ideas for the synthesis of novel organic compounds and polymeric materials. Thanks to the development of various high-pressure equipment and in situ probing technology, the synthesis from simple organic molecules like ethylene and benzene to more complex organic compounds and polymeric materials, such as diamond nanothreads, graphene nanoribbons (GNRs), and graphane, have been achieved. The study of reaction mechanisms under high pressure reveals the widely applied topochemical feature, and the synergistic effect of molecular stacking and thermal vibration in the reaction path, which will enable us to design and synthesize novel functional organic compounds and polymeric materials.

Dynamics and thermodynamics of organics under high pressure

As early as the 1960s and 1970s, scientists tried to apply external pressure to synthesize organic compounds, mainly focusing on the reactions below 1 GPa. The chemical behavior of most compounds at such pressures is not fundamentally different from that at normal pressure, which will not be discussed here.[9] In this section, we mainly focus on the unique behavior of organic systems under pressure well above 1 GPa. From the perspective of thermodynamics, we know that the Gibbs free energy is significantly affected by pressure.[10,11] Quantitatively, in the isothermal process, the change of Gibbs free energy of a compound A from normal pressure (P_O) to high pressure (P_1) can be expressed as $\Delta G_A|_{P_O}^{P_1} = \int_{P_O}^{P_1} dG = \int_{P_O}^{P_1} (V_A dP - S_A dT) = \int_{P_O}^{P_1} V_A dP$, corresponding to the red area in Figure 1a. Similarly, compound B has a change of $\Delta G_B|_{P_O}^{P_1}$, corresponding to the blue area in Figure 1a. The difference between the two is the effect of pressure on the Gibbs free energy change of the reaction "A→B," which can be expressed as $\Delta G_{r,P_1} = \Delta G_{r,P_O} + \Delta G_B|_{P_O}^{P_1} - \Delta G_A|_{P_O}^{P_1}$. Therefore, a reaction involving a decrease in volume may be spontaneous ($\Delta G_{r,P_1} < 0$) at high pressure even if it is non-spontaneous at normal pressure ($\Delta G_{r,P_O} > 0$).[11]

From the perspective of dynamics, Chen et al.[12] first used the concept of activation volume ($\Delta^{\ddagger}V$) to study the behavior of organic systems under high pressure and pointed out that the process with negative $\Delta^{\ddagger}V$ will be accelerated under high pressure, while the process with

DOI: 10.31635/ccschem.024.202405293
Citation: *CCS Chem.* **2025**, 7, 1250–1271
Link to VoR: https://doi.org/10.31635/ccschem.024.202405293

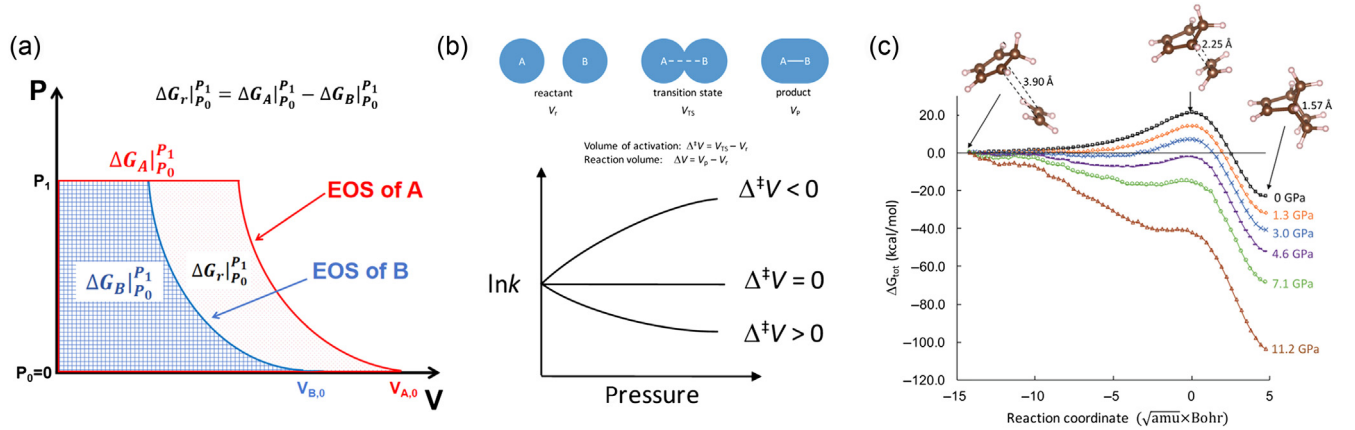

Figure 1 | *(a) Gibbs free energy changes contributed by applied pressure in isothermal process (dT = 0). (b) Typical ln k vs pressure curves for reactions with positive, zero and negative activation volumes. Reprinted with permission from ref 12. Copyright 2017 Wiley-VCH GmbH. (c) Calculated Gibbs energy profiles at different pressures for the Diels–Alder reaction of cyclopentadiene with ethylene. Reprinted with permission from ref 12. Copyright 2017 Wiley-VCH GmbH.*

positive $\Delta^{\ddagger}V$ will be significantly suppressed (Figure 1b). Importantly, diffusion usually has a large positive $\Delta^{\ddagger}V$, which will be greatly suppressed under high pressure. Therefore, the high-pressure chemical reactions often obey the topochemical rules of nearest neighbor priority. Besides, addition polymerization reaction often has a big negative $\Delta^{\ddagger}V$, which is an important reaction type under high pressure. For example, the polymerization barrier of cyclopentadiene and ethylene decreases significantly under high pressure, allowing the reaction to proceed spontaneously and rapidly (Figure 1c).

High-pressure synthesis from organic molecules

The above reaction laws under high pressure are further verified in the reactions of many small molecule systems. This section will briefly describe the high-pressure chemical synthesis from common organic molecules. Alkanes exhibit remarkable stability under high pressure, where the cracking and recombination ($\Delta^{\ddagger}V > 0$) of most alkane molecules occurs only when additional high temperature conditions are applied.[13] This is closely related to the formation and evolution of oil and natural gas in the deep earth, but will not be discussed here.

Ethylene is the simplest unsaturated organic molecule containing double bonds. Wieldraaijer et al.[14] observed the polymerization of ethylene at 2.5 GPa and 330 K using calorimetry without using a catalyst or initiator. Chelazzi et al.[15] discovered that the polymerization paths of ethylene molecules under different pressures were different through the study of reaction kinetics and spectra of the recovered products. At 3.6 GPa, the molecular arrangement in solid ethylene is conducive to the polymerization along a single direction (*a*-axis), and the product is high-density crystalline polyethylene. In contrast, at 5.4 GPa, due to the anisotropic compression of the crystal, the preference along the *a*-axis is destroyed, and branched polymerization is more likely to occur, resulting in low-density polyethylene. This is a good example illustrating that the regulation of molecular packing by pressure is crucial to the structure of the final product.

Acetylene is another typical unsaturated molecule, which polymerizes under the action of Ziegler-Natta catalysts to form a chain with alternating single and double bonds. Above 3.5 GPa, the polymerization occurs at room temperature without a catalyst and produces trans-polyacetylene.[16] At 77 K, acetylene can polymerize into cis-polyacetylene above 11 GPa, which will convert to a trans-structure when heated to room temperature.[17] The high-pressure polymerization of triple bonds is widely applied in the polymerization of a variety of substituted alkyne compounds, such as dicyanoacetylene,[18] diiodoacetylene,[19] acetylenedicarboxylic acid,[20] and so on.

As an unsaturated molecule, the acetonitrile molecule is quite special. At 25 GPa, the methyl group in the molecule is activated and donates the hydrogen atom to the nitrogen atom with the help of intermolecular hydrogen bonds. Finally, a graphitic material is generated and ammonia is released when there is crack in the chamber.[21] The pressure-induced hydrogen transfer phenomenon also occurs in 2-butyne, which first forms 1,3-butadiene via a double CH$\cdots\pi$ aromatic transition state before the polymerization.[22]

Novel materials from high-pressure organic chemical reactions

With an understanding of the reaction laws of organic systems under high pressure, a series of novel polymeric materials have been designed and synthesized, including diamond nanothreads, GNRs, graphane, and so on. The

DOI: 10.31635/ccschem.024.202405293
Citation: *CCS Chem.* **2025**, 7, 1250–1271
Link to VoR: https://doi.org/10.31635/ccschem.024.202405293

method of using high pressure to synthesize these new polymeric materials, is known as pressure-induced polymerization (PIP).

Diamond nanothread is a new type of sp^3-C one-dimensional nanomaterial, which has been a focus over the past decade. One typical structure model was predicted by Stojkovic et al.[23] as early as 2001 and was named as tube (3,0). Subsequently, Xu et al.[24] enumerated up to 50 nanothreads structures derived from benzene. In 2015, Fitzgibbons et al.[25] observed the one-dimensional diamond nanothread in the recovered polymerized benzene after a slow compression experiment. In 2017, Li et al.[26] obtained one-dimensional sp^3-C nanothreads crystals by slowly compressing crystalline benzene, and showed through X-ray diffraction that it has two-dimensional ordered pseudohexagonal packing in the plane perpendicular to the uniaxial pressure, but no ordering was observed in the polymerization direction.

To further investigate the specific structure of benzene nanothreads, Duan et al.[27] used solid-state nuclear magnetic resonance (SSNMR) to conduct a detailed study of ^{13}C-enriched benzene nanothreads, pointing out that the nanothreads formed by benzene under high pressure are a mixture of multiple different structures. Among them, about 20%–45% of benzene is converted into diamond nanothreads with a length of at least 2.5 nm and degree-6 (six atoms of each benzene ring transforms into sp^3-C), but the bonding path is diverse. About one-third of benzene forms diamond nanothreads with isolated double bonds and degree-4, while the degree-2 structure does not exist.

There are many other reports on studying the product structure and the reaction pathways of benzene-derived nanothreads.[28,29] All of them show that benzene has multiple possible reaction pathways under high pressure, including Diels–Alder reactions and para-polymerization and so on, and ultimately forms complex and diverse nanothreads structures. This is because the π–π interaction is too weak to induce suitable stacking for bonding, and the reactivities of the six carbon atoms are similar.

Replacing the carbon in the benzene ring structure with inert heteroatoms like nitrogen, oxygen, and sulfur is a feasible solution for synthesizing more ordered diamond nanothreads. Oxygen and sulfur in the ring do not form any more bonds in the investigated pressure range, and the bonds between nitrogen and nitrogen at high pressures also prove to be extremely demanding and difficult to maintain at atmospheric pressure.[30] Therefore, inert heteroatoms will limit the reaction path of unsaturated organic molecules in the formation of diamond nanothreads, making the product structure more ordered and unique. So far, diamond nanothreads formed by the high-pressure polymerization of furan,[31] thiophene,[32] pyrrole,[33] and pyridazine[34] have been reported, showing more ordered structures than benzene nanothreads.

High-pressure polymerization of s-triazine is also an important example of using heteroatoms to regulate the order of diamond nanothreads. s-Triazines have perfect π–π packing perpendicular to the molecular plane, with the nitrogen in one molecule right against the carbon in the adjacent molecule. Compared to benzene, the presence of nitrogen atoms prevents s-triazine from polymerizing in the conventional [4+2] reaction. Under 10.2 GPa and 575 K, the carbon of s-triazine bonds to the nitrogen of adjacent molecule and forms a perfect tube (3,0) diamond nanothread in a [1,3,5] cooperative addition reaction and the product shows amazing order (Figure 2a). This reaction pathway under high pressure has never been observed before and is named as the "Pericage Reaction."[35]

The packing form of organic molecules also has a significant impact on the polymerization reaction. The unique reaction mode of s-triazine is largely due to its antiphase π–π packing structure. Furthermore, enhancing intermolecular hydrogen bonds or π–π interactions by adding substituting groups, preparing co-crystals, and so on is also an important solution to improve the ordering of diamond nanothreads. Aromatic hydrocarbons and perfluoroaromatic hydrocarbons have opposite quadrupole moments, which results in electrostatic interaction between them and makes their co-crystal in very ordered columnar packing.[36,37] When the pressure increases, the intermolecular distance will be compressed more significantly along the direction of packing, which is conducive to the formation of a one-dimensional diamond nanothread structure.

Another important example is 2,5-furandicarboxylic acid (FDCA). The presence of inert heteroatoms and strong hydrogen bonds gives it high reaction selectivity and a suitable molecular packing structure. By compressing 2,5-furandicarboxylic acid to above 12 GPa, three-dimensional atomically ordered diamond nanothreads were successfully obtained (Figure 2b). The atomic coordinates of the product were directly obtained through Rietveld refinement, which is extremely rare in the field of high-pressure organic synthesis, and the product is determined to be a syn-polyfuran diamond nanothread structure.[38] Dunning et al.[39] also reported a similar study and found that several 3d metals can bind to the backbone, expanding the research of nanothreads in coordination chemistry.

In addition to the above methods, the use of appropriate external stimuli, such as heating,[35] light,[40] and so on, can also effectively reduce the pressure of the polymerization reaction and form a product with better crystallinity. It is also worthy to note that postsynthesis can also be combined with high-pressure synthesis. For the pyridazine nanothreads, heating at 250 °C for 72 h will remove the azo group in its structure as N_2.[34]

In addition to diamond nanothreads, the high-pressure synthesis of GNRs can also be achieved by rationally selecting the structure and packing of the PIP reaction

DOI: 10.31635/ccschem.024.202405293
Citation: *CCS Chem.* **2025**, 7, 1250–1271
Link to VoR: https://doi.org/10.31635/ccschem.024.202405293

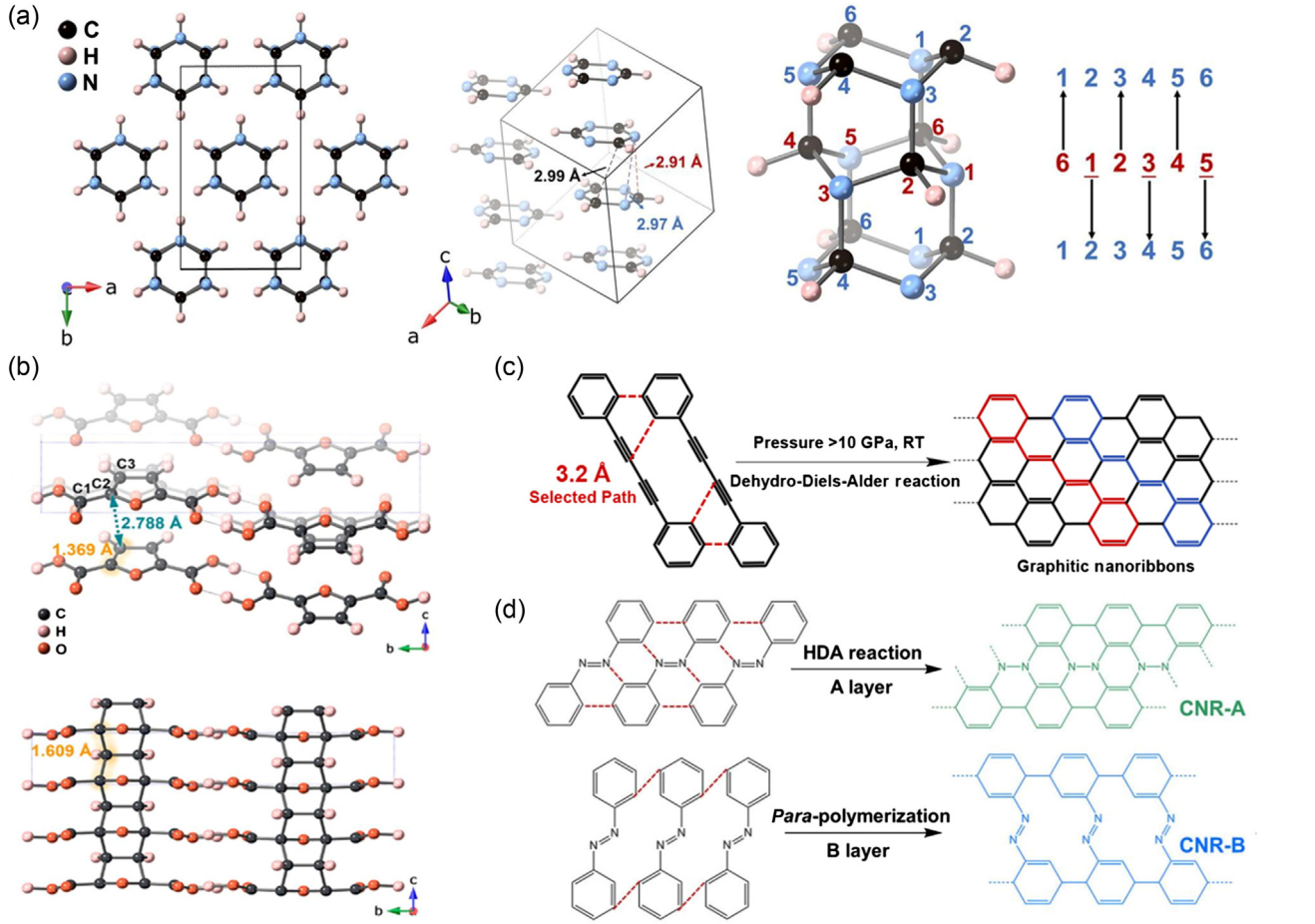

Figure 2 | *(a) Crystal structure of s-triazine at 12.1 GPa and product bonding mode. Reprinted with permission from ref 35. Copyright 2022 National Academy of Sciences. (b) The crystal structure of FDCA at 10.8 GPa and syn-FDCA-CNTh model. Reprinted with permission from ref 38. Copyright 2022 American Chemical Society. (c) Polymerization of DPB under high pressure. Reprinted with permission from ref 41. Copyright 2020 American Chemical Society. (d) Polymerization of Azobenzene under high pressure. Reprinted with permission from ref 43. Copyright 2023 American Chemical Society.*

precursors. GNRs are quasi-one-dimensional carbon nanomaterials, referring to graphene strips with a width of less than 50 nm, and are considered to be a feasible solution to open the zero band gap of graphene materials, which have potential application value in fields such as electronic devices and optical communication system. In 2020, Zhang et al.[41] reported for the first time the construction of crystalline GNRs using 1,4-diphenylbutadiyne (DPB) as a precursor, further expanding the synthesis strategy of GNRs. This process is a dehydro-Diels–Alder (DDA) reaction with phenylethynyl as the diene and phenyl as the dienophile, which is also the first report in the field of high-pressure synthesis (Figure 2c). 1,3,5-Triethynylbenzene (TEB) also has a similar reaction mode. At 4 GPa, the phenyl and alkynyl groups in TEB simultaneously participate in the DDA reaction to form an sp^2/sp^3 hybridized nanoribbon structure.[42] Azobenzene can also generate a carbon nanoribbon structure through [4+2] hetero-Diels–Alder or para-polymerization reaction under high pressure. Due to the existence of two different molecular packings in its crystal, it will produce a unique van der Waals carbon nanoribbon heterojunction structure under high pressure (Figure 2d).[43]

Graphane is formed when all carbon atoms of graphene are saturated with hydrogen. With different attacking directions of hydrogen (above or below the graphene plane), many polymorphs with combinations of chair/boat configurations are expected. However, the traditional hydration process could not generate graphane with specific configurations. In 2017, Sun et al.[44] found the high-pressure synthetic route from acetylene to short-range ordered graphane-II via cis-polyacetylene. This conclusion was confirmed by SSNMR and neutron pair distribution function.

The high-pressure polymerization of benzene-hexafluorobenzene cocrystal also produced graphane. The product has an ordered hydrogen-fluorine-substitution, which cannot be achieved via other synthetic methods.

DOI: 10.31635/ccschem.024.202405293
Citation: *CCS Chem.* **2025**, 7, 1250–1271
Link to VoR: https://doi.org/10.31635/ccschem.024.202405293

Table 1 | *Threshold Distances for PIP of Different Organic Molecules at Room Temperature*

Organic Molecule	$d_{(C\cdots C)min}$ (Å)	Critical Pressure (GPa)	Functional Group
Acetylene[44]	3.1	5.7	Alkynyl
Acetylene dicarboxylic acid[20]	3.1	8	Alkynyl
Benzene[25]	2.8	18	Phenyl
Benzene-hexafluorobenzene[45]	2.8	20	Phenyl
Azulene[47]	2.9	15	Azulene
2,6-Diethynylpyridine[48]	2.9	4	Alkynyl, Pyridine
1,4-Diphenylbutadiyne[41]	3.2	10	Alkynyl, Phenyl
1,3,5-Triethynylbenzene[42]	3.4	4	Alkynyl, Phenyl

Under high pressure, the cocrystal undergoes multiple phase transitions and eventually forms a tilted columnar structure, which indicates that the π–π interaction between molecules is not sufficient to maintain the stability of the structure under high pressure. The cocrystal experiences several steps of reaction and finally forms a short-range ordered structure of graphane-III.[45]

There have been many reports on the PIP reactions of unsaturated organic molecules, but we also need to note that not only unsaturated molecules can be used for PIP reactions. An important example is that Huang et al.[46] used saturated cubane molecules as precursors to generate the smallest carbon nanothread structure through molecular strain-driven polymerization.

Mechanism of high-pressure organic synthesis

As mentioned above, the topochemical reaction is highly preferred under high pressure; therefore, the geometric parameters inside the crystal before reaction become extremely important. In Table 1, we summarized the critical pressure and critical C · · · C distance required for some organic molecules to bond at room temperature. The critical pressure for the PIP reaction in different systems varies greatly, but the same functional groups often start to bond at similar critical C · · · C distances.

As early as 2007, Ciabini et al.[49] explored the relationship between the critical distance and the reaction of crystalline benzene, and proposed that the polymerization of benzene is related to the shortest instantaneous molecular distance in the system, which is called the intrinsic critical distance (d_{intr}). To further explore the chemical laws corresponding to the critical C · · · C distance, Tang et al.[50] calculated and analyzed the molecular dynamics, phonon spectrum, and polymerization transition state of acetylene crystals under high pressure, and proposed a reaction model in which the empirical critical distance (3.1 Å) equals the sum of the intrinsic critical distance (2.3 Å) and the thermal vibration contribution

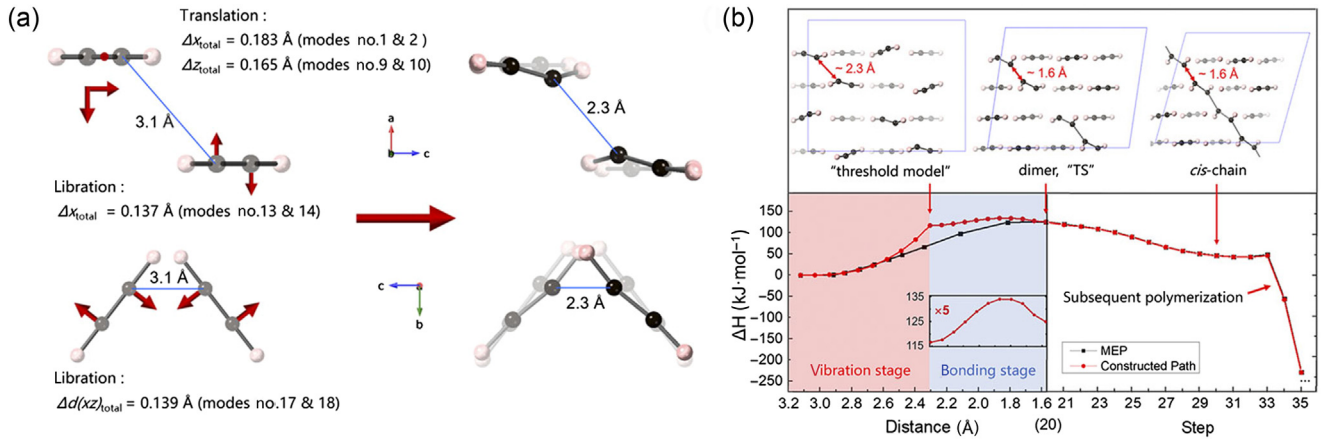

Figure 3 | *(a) Vibrational displacement of carbon atoms from the equilibrated position with T-point symmetry applied. The instantaneous $d_{C\text{-}C}$ at room temperature (RT) becomes 2.3 Å and reaches the threshold for intermolecular bonding. (b) Reaction curve from acetylene to polyacetylene in the crystal. The minimum energy path (MEP) is shown as the black line, and the pathway through the transient "threshold model" is shown as the red line. Reprinted with permission from ref 50. Copyright 2023 Matter and Radiation at Extremes.*

DOI: 10.31635/ccschem.024.202405293
Citation: *CCS Chem.* **2025**, 7, 1250–1271
Link to VoR: https://doi.org/10.31635/ccschem.024.202405293

(0.8 Å). This model well explains the underlying laws behind the threshold distance of PIP reactions and provides strong theoretical support for the design and synthesis of new organic compounds under high pressure (Figure 3a,b).

High-Pressure Synthesis of Novel Inorganic Compounds

High-pressure synthesis of inorganic materials, mostly accompanied by simultaneous high temperatures, has significantly accelerated the discovery of new inorganic compounds with exotic structures and properties that cannot be obtained at ambient pressure.[51,52] So far, a considerable number of compounds, including but not limited to hydrides, borides, carbides, nitrides, chalcogenides, and halides, have been prepared by either multianvil presses or diamond anvil cell apparatus. A screening of the achievements in inorganic compounds synthesized under high-pressure is highly desired to unveil the laws of atomic-scale phase engineering for desired properties, highlight the emerging trends and challenges, and accelerate the materials exploration process by structure-function oriented precise prediction and inverse design.

Chalcogenide and halide

Inorganic oxides and chalcogenides (sulfur, selenium, and tellurium) are central to the study of solid functional materials involved in almost all aspects of materials science research. The exploration of high-pressure synthesis of inorganic oxides/chalcogenide has greatly enriched chemical space of such compounds. Oxides are among the most common and widely applied materials, such as the perovskite-related family in general chemical formula ABO_3, and exhibit a key focus of multifunctional materials due to their high chemical flexibility and wide range of structural variants.[52,53] For examples, the perovskite-related Ruddlesden–Popper (R–P) $La_3Ni_2O_7$ phase undergoes a structural phase transition from *Amam* to *Fmmm* under high pressure, yielding a significant breakthrough of superconducting transition temperature (T_c) above 80 K at 14 GPa.[54] High-pressure and high-temperature conditions allow the development of unique synthetic pathways to incorporate small transition metal ions into both the *A* and *B* sites of perovskites for rare polar magnets or quantum magnetoelectric materials.[55,56] For example, the *R*3-Mn_2MnWO_6 synthesized at 8 GPa and 1673 K demonstrates an antiferromagnetic transition at 58 K and high spontaneous polarization of ~63.3 μC-cm^{-2}. Its spontaneous polarization significantly increases near the magnetic ordering temperature, which implies intrinsic magnetoelectric coupling (Figure 4a).[57] The crystal and local structure of these exotic perovskites can be highly chemically and thermodynamically dependent. For instance, Mn_2FeReO_6 (5–8 GPa and 1573 K), in contrast, adopts the monoclinic ($P2_1/n$) symmetry other than the polar *R*3 analog, and exhibits a positive giant magnetoresistance up to 220% at 5 K under 8 T magnetic field.[58,59] In addition, the *A*-site ordered quaternary perovskite $AA'_3B_4O_{12}$ provides more chemical and crystallographic freedom for high-pressure and high-temperature synthesis.[60] The *A*- and *B*-site-ordered $LaCu_3Fe_2Re_2O_{12}$ (9 GPa and 1273 K) holds the record for the experimentally highest Curie temperature (710 K) reported in perovskite-type half-metals, a breakthrough in high-temperature semimetallic oxides with a spin-down conduction band and a spin-up of 2.27 eV (Figure 4b).[61] These findings open a new platform for the exploration of novel magnetoelectric materials for spintronic applications.

Since the discovery of superconductivity in iron-based dopants, low-dimensional chalcogenide superconductors have become a hot spot in screening superconductors. Pressure is an effective parameter to regulate the inter or intrachain distance and thus modify the atomic interactions and band structure, resulting in unique electronic and structural properties. Through high-pressure techniques, many low-dimensional chalcogenide superconductors, such as HfS_3, SnS_2, and HgS, have been discovered and reported one after another.[62–64] HfS_2 has attracted much attention due to its complex electronic phase transition. At 15 GPa, HfS_2 undergoes a structural phase transition from *P*-3*m*1 to *Immm*, and further ramping up to 43 GPa results in another structural transition to *I*4/*mmm*. There is also a phase transition from *I*4/*mmm* to *R*-3*m* at low temperatures. HfS_2 undergoes a semiconductor-to-metal electronic phase transition at 68.6 GPa. Zero resistance was observed at 147 GPa at 1.7 K, and a superconducting state with T_c of 16.4 K at 158 GPa—the highest reported T_c among transition-metal dichalcogenides to date.[65,66] Similarly, $CrSbSe_3$ exhibits a ferromagnetic ordering at 71 K and ambient pressure. It undergoes an insulator-to-metal transition at 32.8 GPa, followed by a structural change and superconductive response at 57.9 GPa (Figure 4c,d). Researchers attribute this continuous electronic transition to the enhanced p-d hybridization between Se and Cr, which leads to adjustments in the electronic structure under compression.[67] High-pressure studies of chalcogenides not only reveal significant structural transformations, but also highlight their immense potential for superconductivity. These findings extend the understanding of the physical properties of chalcogenide under extreme conditions and provide valuable insights into the design and discovery of novel superconducting materials.

Two-dimensional metal halides have attracted much attention as quantum materials. Among them, α-$RuCl_3$ is considered to be one of the most promising candidates for the realization of Kitaev quantum spin liquid (QSL).

DOI: 10.31635/ccschem.024.202405293
Citation: *CCS Chem.* **2025**, 7, 1250–1271
Link to VoR: https://doi.org/10.31635/ccschem.024.202405293

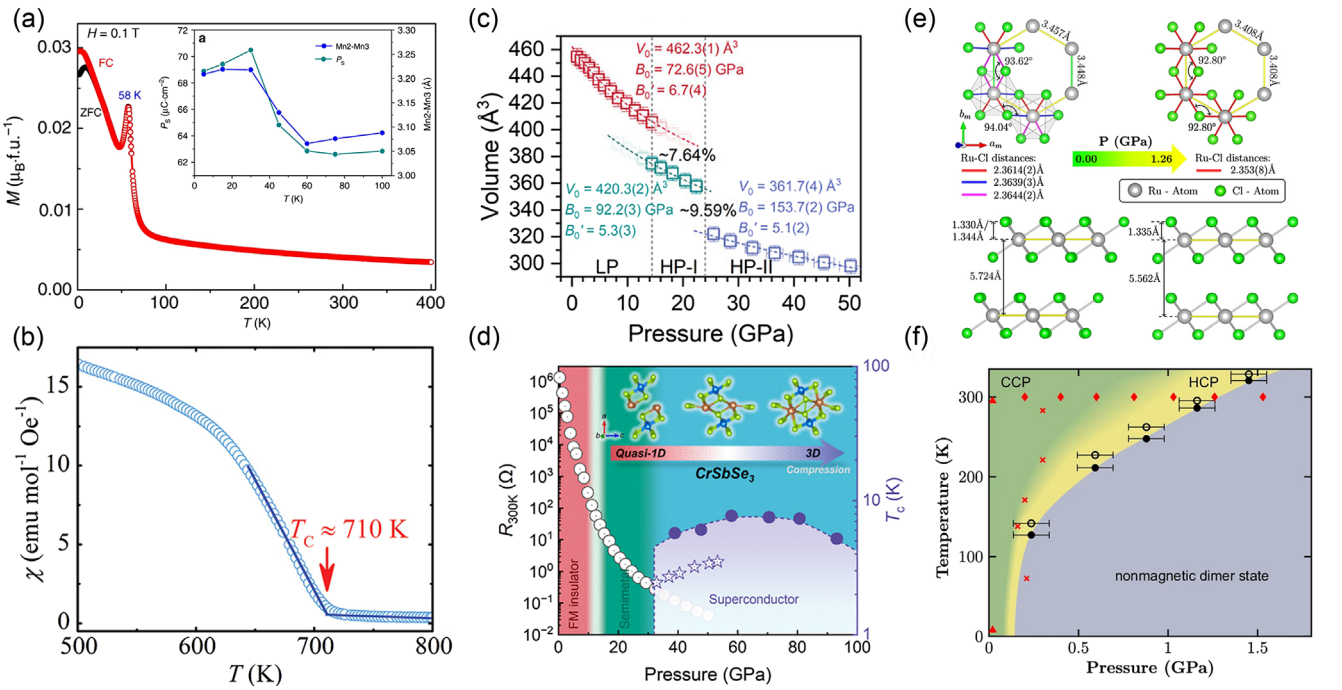

Figure 4 | *(a) The magnetization (M)-temperature (T) curve of Mn_2MnWO_6 at H = 0.1 T external field. The inset is the spin-polarization-temperature profile. Reprinted with permission from ref 57. Copyright 2017 Nature Publishing Group. (b) Magnetic transition temperature of $LaCu_3Fe_2Re_2O_{12}$ determined by the tangent method at 710 K. Reprinted with permission from ref 61. Copyright 2022 Wiley-VCH GmbH. (c) Pressure-volume evolution curves and (d) superconducting phase diagrams of $CrSbSe_3$. Reprinted with permission from ref 67. Copyright 2024 American Chemical Society. (e) Schematic crystal structure evolution at high pressure, and (f) temperature-pressure phase diagram of $RuCl_3$. Reprinted with permission from ref 68. Copyright 2024 Nature Publishing Group.*

High-pressure and high-temperature treatment rearranges its honeycomb layer, resulting in the formation of a highly symmetric triangular structure (Figure 4e), which leads to a high Kitaev-to-Heisenberg exchange ratio (K/J) up to 124, and provides a new perspective for QSL research (Figure 4f).[68] Both α-$RuBr_3$ and α-RuI_3 require high-pressure and high-temperature synthesis to form the two-dimensional honeycomb feature similar to those of α-$RuCl_3$.[69,70,71] It is noteworthy that α-$RuBr_3$ shows long-range magnetic ordering at 34 K, which suggests that the Kitaev interactions in α-$RuBr_3$ are weaker than those in α-$RuCl_3$.[69] In contrast, α-RuI_3 behaves significantly different, exhibiting metallic properties and Pauli paramagnetic, which may be due to increased electron precipitation from iodine.[72]

The structural changes of halides under high-pressure conditions are often accompanied by lattice reduction and shorter interatomic distances, which in turn affect the electronic structure and optical properties. For example, NH_4Cl experiences two phase transitions under high pressure, shifting from the original *Pm-3m* to *P43m*, and then to *P42m*, along with a unique "off-on-off" second harmonic generation (SHG) switching behavior (Figure 5a). This "on-off-on" SHG signal phenomenon marks the first observation of such a three-state SHG switching in a single material.[73] Pressure can also effectively regulate the energy band size in halides. The double perovskite $Cs_2AgBiBr_6$ shows promising optoelectronic properties, such as a small effective carrier mass and long carrier lifetime. However, the relatively large band gap (2.2 eV) hinders its use in optoelectronic devices. While under high pressure, $Cs_2AgBiBr_6$ undergoes a structural phase transition from the cubic to tetragonal phase, with tilting and deformation of the $AgBr_6$ and $BiBr_6$ octahedra, leading to a significant increase of the band gap. When pressure exceeds 6.5 GPa, the structure further transforms into an amorphous state, causing significant bandgap narrowing to 1.7 eV (Figure 5b).[74] Additionally, the one-dimensional metal halide $CsCu_2I_3$ contains $[CuI_4]^{3-}$ tetrahedral units. This low-dimensional structure enhances quantum confinement effects and promotes the formation of self-captured excitons. $CsCu_2I_3$ undergoes a structural phase transition from the orthorhombic symmetry to the high-pressure orthorhombic phase upon pressing, which is accompanied by a significant enhancement of the emission intensity of the self-trapped excitons, resulting in an intense yellow luminescence (Figure 5c). This

DOI: 10.31635/ccschem.024.202405293
Citation: *CCS Chem.* **2025**, 7, 1250–1271
Link to VoR: https://doi.org/10.31635/ccschem.024.202405293

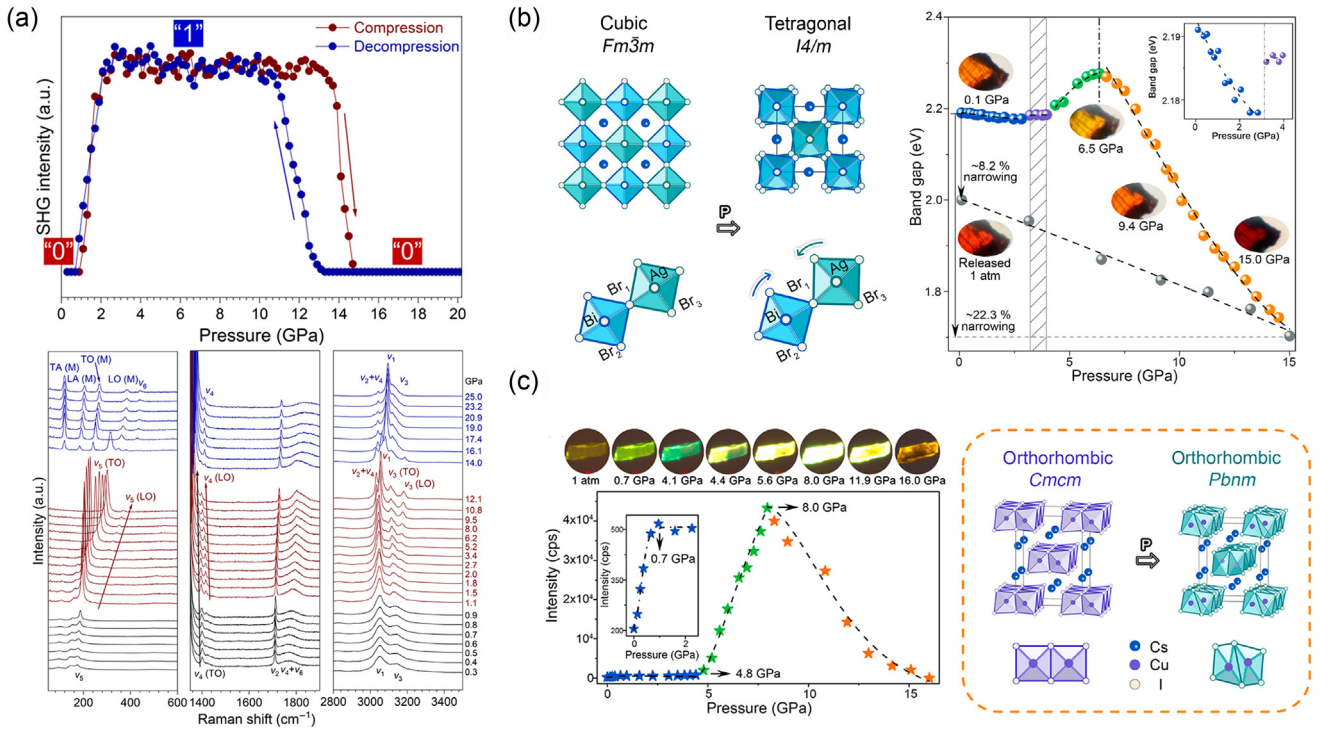

Figure 5 | *(a) SHG intensity vs pressure and Raman spectral evolution during pressurization of powder NH_4Cl. Reprinted with permission from ref 73. Copyright 2024 American Chemical Society. (b) Schematic structural evolution and bandgap evolution curve under pressure of $Cs_2AgBiBr_6$. Reprinted with permission from ref 74. Copyright 2023 American Chemical Society. (c) PL micrographs of $CsCu_2I_3$ crystals during compression and the corresponding changes in the maximum intensity of self-captured exciton emission, and a schematic of the structural evolution of $CsCu_2I_3$ during compression. Reprinted with permission from ref 74. Copyright 2023 American Chemical Society.*

enhancement is attributed to the increase in tetrahedral distortion and the promotion of tetrahedral tilting within the chain.[74]

Nitride, phosphide, boride, and hydride

Nitrides have a wide range of potential applications in electronics, optics, and energy storage due to their unique electronic structure and chemical stability.[75] Simple metal nitrides synthesized under high pressure have shown impressive performance in superhard materials. For example, by heating Re and ammonia or ammonium azide at 40–90 GPa and 2200–2500 K, researchers synthesized $Re_2(N_2)(N)_2$, which possesses an exceptionally high bulk modulus (K_0 = 428 GPa) and hardness (nanoindentation hardness of 36.7 GPa).[76] Similarly, a novel hexagonal nitride with *P*-6*m*2 symmetry (Pearson symbol: *h*P2), $WN_{1-\delta}$, was recently synthesized using high-pressure techniques. This compound was formed by reacting WCl_6 with $NaNH_2$ at 3 GPa between 1473 and 1673 K. The actual composition of $WN_{1-\delta}$ is $WN_{0.764}$. This non-stoichiometric composition helps stabilize its crystal structure. $WN_{1-\delta}$ exhibits excellent mechanical properties and thermal stability, with hardness and bulk modulus comparable to, and in some aspects, exceeding those of tungsten carbide (WC) (Figure 6a).[77]

Additionally, more complex multinary nitrides have also be synthesized under high pressure. For instance, Kawamura et al.[78] reported the successful synthesis of a novel rock-salt-type nitride semiconductor, $MgSnN_2$, through a substitution reaction at 5.5 GPa and 1123 K. $MgSnN_2$ has an estimated bandgap of 2.3 eV and displays distinct cathodoluminescence peaks at room temperature (Figure 6b,c). Weidemann et al.[79] reported the high-pressure synthesis of three single-layer R–P (K_2NiF_4-type) nitrides: Pr_2ReN_4, Nd_2ReN_4, and Ce_2TaN_4 (8 GPa and 1273 K). Pr_2ReN_4 and Nd_2ReN_4 were synthesized from the corresponding rare-earth nitrides, Re powder, and NaN_3 under high-pressure conditions. Pr_2ReN_4 exhibits metallic behavior with low residual resistivity, while Nd_2ReN_4 shows semiconducting characteristics, which may be a result of grain boundary effects.[79] These studies not only enrich our understanding of high-pressure phase diagrams but also provide a theoretical foundation for the future experimental synthesis of novel nitrides.

Research on the high-pressure synthesis of phosphides is an active and challenging field. Limited phosphorus-containing materials with unique physical and chemical

DOI: 10.31635/ccschem.024.202405293
Citation: *CCS Chem.* **2025**, 7, 1250–1271
Link to VoR: https://doi.org/10.31635/ccschem.024.202405293

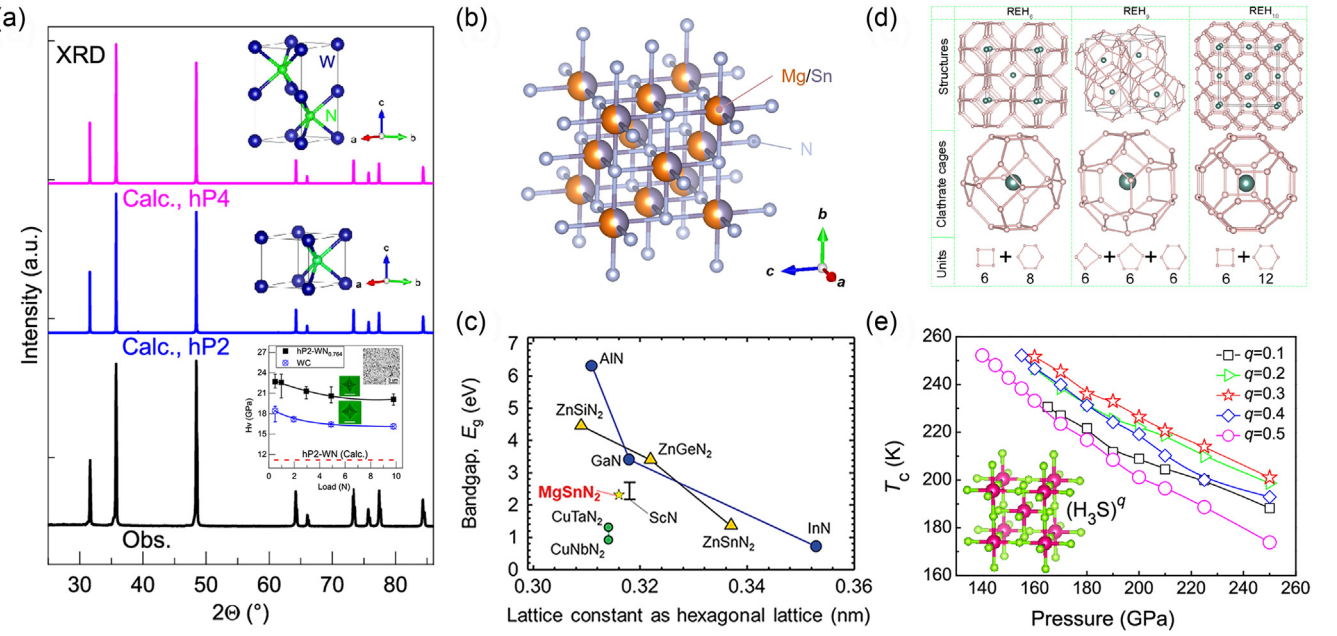

Figure 6 | *(a) Comparison of the experimental and simulated X-ray diffraction patterns (XRD) of $WN_{1-\delta}$. The inset shows the comparison curves of $WN_{1-\delta}$ and WC in hardness. Reprinted with permission from ref 77. Copyright 2024 American Chemical Society. (b) Schematic structure of $MgSnN_2$ and (c) comparison of energy bands of several nitrides. Reprinted with permission from ref 78. Copyright 2020 Wiley-VCH GmbH. (d) Schematic structures of REH_6, REH_9, and REH_{10} (RE: Rare Earth). The small spheres indicate that the hydrogen atoms form a cage-like structure surrounding the large rare earth atoms. Reprinted with permission from ref 90. Copyright 2017 American Physical Society. (e) Pressure-dependent T_c evolution of hole-doped H_3S. Reprinted with permission from ref 93. Copyright 2022 American Chemical Society.*

properties have been discovered to show potential applications for superhard, magnetic, and electronic materials. For instance, Ir_2P, a cubic phosphide synthesized under high-pressure and high-temperature conditions, crystallizes in *Fm*-3*m* space group and also exhibits a high bulk modulus. In situ high-pressure test shows that Ir_2P has a bulk modulus, B_0, of 306(6) GPa and hardness of 11.8(4) GPa. However, theoretical calculations suggest a relatively low shear modulus about 64 GPa, indicating complex overall bonding in Ir_2P, combining metallic, ionic, and covalent characteristics. Magnetic susceptibility measurements revealed that Ir_2P exhibits spin-glass behavior.[80] The layered GeP_5 (2 GPa and 1273–1500 K) also displays superconductivity. In situ electrical transport measurements under high pressure show that in GeP_5 the superconducting transition temperature reaches a maximum of 10.5 K at 13.5 GPa. Remarkably, this superconductivity remains robust up to 60 GPa, without any significant decrease. This pressure-induced superconductivity is likely related to the pronounced softening of phonon modes, associated with the extension of in-plane P–P bonds in the GeP structure.[81]

The mechanical and electronic properties of borides can be effectively modified by adjusting the pressure. For instance, the orthorhombic MnB (5 GPa and 1600–2200 K) with a FeB-type structure (*Pnma*) exhibits excellent room-temperature ferromagnetism and high hardness. Its magnetic Curie temperature reaches as high as 546.3 K and asymptotic Vickers hardness is as high as 15.7 GPa. MnB combines excellent mechanical and fantastic magnetic properties, showing potential industrial applications.[82] The discovery of superconductivity in MgB_2 evokes extensive exploration in borides with similar structures or compositions. However, only a few compounds demonstrate superconductivity with relatively low T_c among approximately 100 binary borides explored. Pei et al.[83] reported that MoB_2 exhibits superconductivity with a T_c up to 32 K under high pressure, the highest T_c discovered in transition metal borides to date. Theoretical calculations suggest that the T_c of MoB_2 can be well-explained within the electron-phonon coupling framework, with the coupling between Mo d-electrons and out-of-plane Mo phonon modes, being the primary driver of its 32 K superconductivity.[83] These findings open up new avenues for exploring high-T_c superconductors within the realm of transition metal borides.

At extremely high pressure, atomic distances are compressed, driving a state distinct from that at ambient or low pressure. This has sparked a wave of research into hydride superconductors. In 2015, Eremets et al.[84] synthesized superconducting H_3S with high-T_c of 203 K through high pressure and high temperature. In fact, the

DOI: 10.31635/ccschem.024.202405293
Citation: *CCS Chem.* **2025**, 7, 1250–1271
Link to VoR: https://doi.org/10.31635/ccschem.024.202405293

precursors of hydrides are important to the successful synthesis of high-T_c hydride superconductor.[85–87] Ma et al. successfully prepared a clathrate CaH_6 superconductor with T_c up to 215 K by using BH_3NH_3 as one of starting precursors,[88] even after 10 years from the first theoretical prediction.[89] Building on the characteristic hydrogen cage structure of CaH_6, researchers further explored rare-earth hydrides with variable hydrogen content under high pressure, and summarized the general trend of extraordinarily high T_c in cage-like hydrides (Figure 6d).[90] Typical high-pressure synthesis of high-T_c superconducting clathrate hydrides goes to the LaH_{10} from experiments[91] and theoretical prediction.[92] H_3S, has significantly advanced the prospect of room-temperature superconductors under high pressure. According to theoretical calculations, H_3S exhibits four crystal phases under different pressures, including *P*1 (below 37 GPa), *Cccm* (37–111 GPa), *R3m* (111–180 GPa), and *Im*-3*m* (180–300 GPa). The T_c of hole-doped H_3S can be further enhanced to 253 K at 140 GPa (Figure 6e).[93] The superconducting mechanism in hydrides is often closely related to electron-phonon coupling. The low mass of hydrides increases phonon frequencies, which in turn enhances electron-phonon coupling and induces the high T_c characteristics. In contrast, XeH_{14}, compressed to 300 GPa, did not exhibit high superconducting T_c, since the hydrogen atoms did not form a cage structure. This illustrates that merely having a high hydrogen content is insufficient to achieve high T_c superconductivity by high pressure synthesis. Hydrogen must form a specific cage-like structure to contribute to superconductivity under high pressure.

The way to precise high-pressure inorganic synthesis

High-pressure synthesis of new inorganic materials not only provides insights into fundamental scientific questions, but also holds immense potential for industrial innovation. In the past decades, high pressure techniques have become a powerful tool to synthesize materials that cannot be obtained under ambient conditions. However, the high cost and complex operations involved in high-pressure experiments have significantly hindered their widespread adoption. Therefore, a precise and universal theoretical prediction is highly desired to accelerate the precise discovery of new functional materials with minimal cost.[94] The Murnaghan Equation of State (EOS) is an empirical formula used to describe the volume changes of solids under high pressure.[95] It is widely applied, particularly in high-pressure physics and materials science, to approximate the compressibility of materials and their response to pressure. In combination with an EOS, first-principles density functional theory calculations, big-data mining, and high throughput computing can map out the dependence of a material's relative enthalpy or energy with pressure, which can somehow accurately predict the stability of different polymorphs under different pressures. This approach has already been validated in materials synthesized under high pressure. By summarizing and analyzing the structures of known materials with general formula, it is possible to significantly narrow down the potential crystal structures of target materials. Further analysis can effectively predict the crystalline structure, synthesis conditions, and related physical and chemical properties of target materials that have not yet been synthesized.

The paradigm of "big-data mining-high-throughput learning and prediction-targeted synthesis" has accelerated the efficient high-pressure synthesis of unknown materials. For example, by mining and analyzing existing databases of compounds with a general chemical formula of $Li_2BB'O_6$, 140 candidate materials were identified through learning and screening. Further refined analysis resulted in 10 target compounds with synthesis potential, ultimately guiding the successful synthesis of nonmagnetic Li_2TiTeO_6 under 6 GPa and 1123 K.[96] In more complex magnetic systems like A_3TeO_6 (*A* = Mg, Mn, Fe, Co, Ni, Cu, Zn), this theoretical prediction paradigm also successfully guided the discovery of the multiferroic *R*3-Co_3TeO_6 (5 GPa and 1223 K).[97] In subsequent studies, this predictive model was further validated in the Ag_2B(IV)B'(VI)O_6 system, verifying its accuracy and universality across the entire pressure range, from negative to high positive pressure, as well as in magnetic and nonmagnetic systems.[98] These findings speak for the powerful potential of data-driven predictive models in materials science, particularly in discovering and designing novel multifunctional high-pressure metastable materials. With experimental validation, these predictions can not only guide future research but also methodologically accelerate the development of new materials.

The Retention of High-Pressure Phase

High-pressure chemistry has provided a huge boost to the development of scientific community. Pressure-induced emission (PIE) in halide perovskites is gradually showing its unique charm in both pressure sensing and optoelectronic device applications.[99–102] Although the PIE in halide perovskites has greatly alleviated the problem of low luminous efficiency to a certain extent, the high-pressure reversibility still largely limits the practical applications.[103,104] Increasing the potential barrier of phase transition is the key to quench the high-pressure phase.[105–107] Thus far, three strategies have been developed to increase the potential barrier of phase transition for achieving the high-pressure phase retention including the nano-size effect, steric hindrance effect, and hydrogen bonding cooperativity effect. Note that these three

DOI: 10.31635/ccschem.024.202405293
Citation: *CCS Chem.* **2025**, 7, 1250–1271
Link to VoR: https://doi.org/10.31635/ccschem.024.202405293

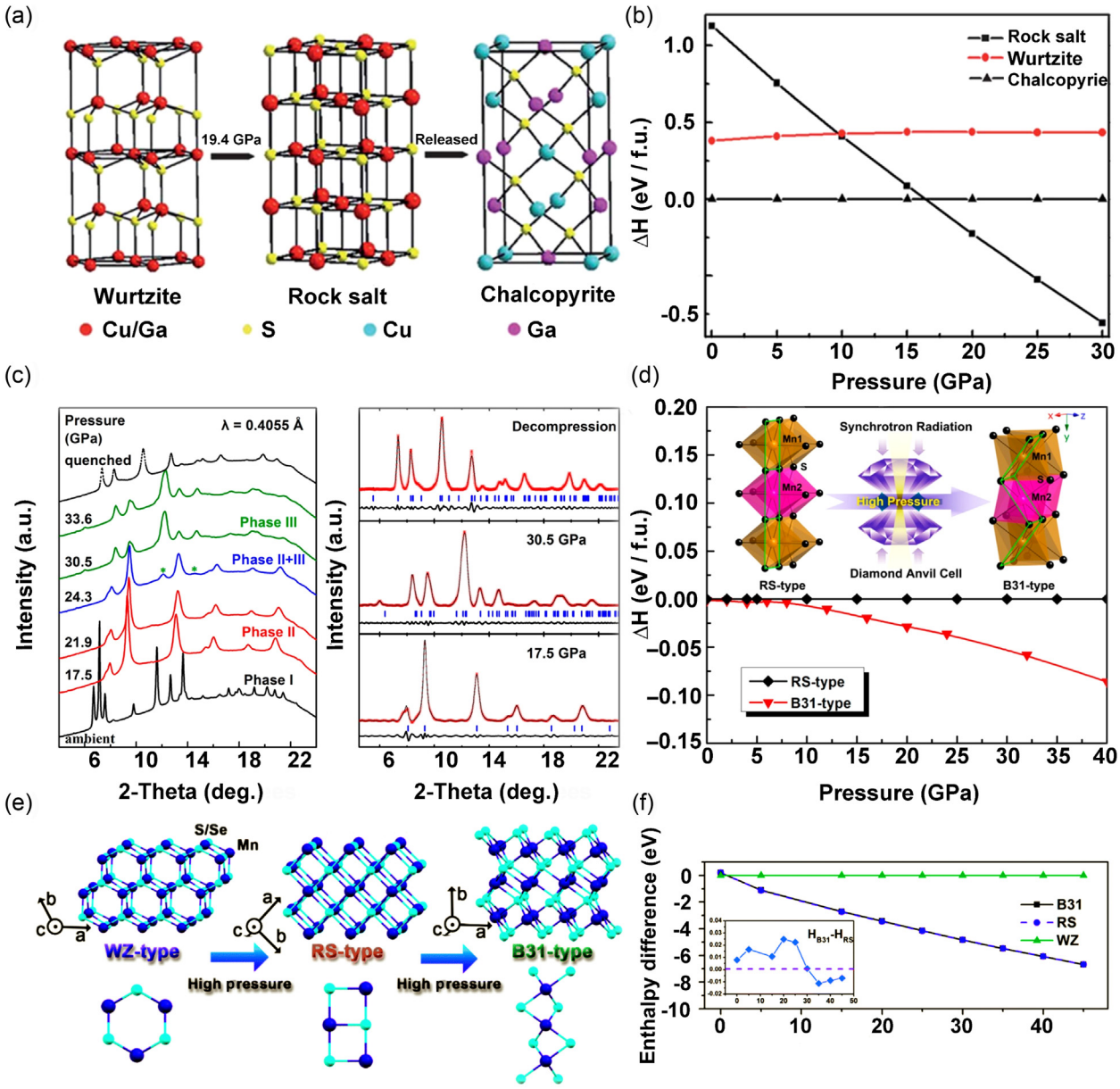

Figure 7 | *(a) Schematic model for the transition of $CuGaS_2$ NCs under compression. Reprinted with permission from ref 110. Copyright 2012 The Royal Society of Chemistry. (b) Enthalpy curves (relative to chalcopyrite structure) per $CuGaS_2$ formula unit of WZ and RS structures as function of pressure in $CuGaS_2$. Reprinted with permission from ref 110. Copyright 2012 The Royal Society of Chemistry. (c) In situ high-pressure synchrotron XRD patterns and Rietveld refinements of WZ-MnS nanorods under high pressure. Reprinted with permission from ref 111. Copyright 2015 American Chemical Society. (d) Pressure dependence of calculated enthalpy differences per formula unit for orthorhombic B31-type MnS relative to cubic RS-type MnS. Inset on the top panel shows the schematic illustration with respect to polyhedral views crystal structures of RS-type and B31-type MnS under high pressure. Reprinted with permission from ref 111. Copyright 2015 American Chemical Society. (e) Unit-cell schematics of MnS (Se) with* P63mc, Fm3m, *and* Pnma *crystal structures under high pressure. Reprinted with permission from ref 112. Copyright 2021 The Royal Society of Chemistry. (f) Enthalpy calculations and pressure-induced atomic motions. Reprinted with permission from ref 112. Copyright 2021 The Royal Society of Chemistry.*

DOI: 10.31635/ccschem.024.202405293
Citation: *CCS Chem.* **2025**, 7, 1250–1271
Link to VoR: https://doi.org/10.31635/ccschem.024.202405293

effects may synergistically affect the ultimate retention of the targeted high-pressure phase.

High-pressure phase retention: nano-size effect

More than a decade ago, advanced nanocrystal (NC) synthesis techniques created the opportunity to prepare metastable materials at nanoscale.[108,109] However, researchers still lacked a reliable understanding of metastable structures. At that time, the high-pressure research of metastable NCs was still in its infancy. Zou and coworkers[110] studied metastable wurtzite-structured $CuGaS_2$ NCs by means of high-pressure techniques. High-pressure experiments and theoretical calculations showed that $CuGaS_2$ underwent a structural transformation from wurtzite (WZ) to rock salt (RS) under pressure. Upon release of pressure, the sample was converted into the energetically more favorable chalcopyrite structure (Figure 7a). Compared with the chalcopyrite structure, the WZ structure has obvious energy defects (0.38 eV/f.u.), which is the reason why the bulk form of WZ structure does not exist (Figure 7b). The key to the stability of the WZ structure at the nanometer scale is the surface effect. The pressure regulated the stability of different phases and also proved that the WZ structure is metastable compared with chalcopyrite structure.

Before long, the nanostructured new phase associated with orthorhombic MnP-type (B31) MnS was excavated out by utilizing an effective high-pressure technique. Zou and coworkers[111] mainly studied the structural changes of salt rock phase of MnS nanocrystalline under high pressure and even after pressure relief. High-pressure synchrotron X-ray diffraction experiments demonstrated that RS-MnS underwent a phase transition at 24.3 GPa, and the new structure was confirmed to be B31 phase (Figure 7c). Interestingly, the structure of MnS NCs did not recover RS phase after pressure relief, but the high-pressure B31 phase was retained. The apparent decrease in the enthalpy of the B31 phase after roughly 10 GPa indicated that B31-type MnS was more energetically preferable under high pressure (Figure 7d). On the contrary, the bulk RS-MnS underwent a completely reversible phase transition after pressure treatment. the unique nanostructures of MnS NCs and the inevitable thermodynamic influence should be responsible for the retention of high-pressure new phase by aggravating the fluctuation of the subtle enthalpy differences under atmospheric pressure.

In the last few years, Zou and coworkers[110] undertook a study on the high-pressure phase transition behaviors of heterostructured core/shell MnSe/MnS nanorods, especially focusing on the new-phase retention engineering of core/shell nanostructures. High pressure could trigger the transition from WZ to RS to B31 phase in the core/shell MnSe/MnS nanorods (Figure 7e), and high-pressure B31 phase was also retained to ambient conditions. First-principles calculations indicated that B31-MnS and MnSe are thermodynamically stable under high pressure, and can survive under ambient conditions owing to the synergistic effect of subtle enthalpy differences in RS and B31 phases and high surface energy in nanomaterials (Figure 7f). So far, the nanosize effect, and low formation enthalpy of high-pressure metastable phase have been verified to increase the barrier of phase transition, thus achieving the purpose of preserving the high-pressure phase.

High-pressure phase retention: steric hindrance effect

In addition to the interception of high-pressure metastable phases, the retention of high-pressure phases with excellent optical properties is also extremely important for practical optoelectronic applications under environmental conditions. The PIE of halide perovskites or derived hybrid metal halides has attracted much attention.[113–116] However, the soft nature of their inorganic lattice makes it challenging for the intense emission within the high-pressure structure to survive under ambient conditions.[117] In recent studies, high-pressure phases with excellent optical properties have been repeatedly captured in organic-inorganic hybrid perovskites containing complex organic macromolecules. The PIE retention is undoubtedly another landmark achievement after PIE. Organic functional groups in perovskite materials may introduce a large amount of steric hindrance under pressure as a buffer layer to adapt to a wide range of pressure, thus changing the pressure point of phase transition and amorphous. This method of introducing steric hindrance to improve the phase transition barrier has been paid attention to by Li et al. as early as 2012.[118,119]

Until 2021, the organic-inorganic hybrid perovskite $(PEA)_2PbCl_4$ NCs (PEA = $C_8H_{12}N$) yielded enhanced cold white light after pressure treatment (Figure 8a), allowing researchers to realize that high-pressure phases in perovskite could be intercepted by the introduction of organic macromolecules.[120] In other words, a complex configuration of organic molecules is introduced to create a steric hindrance, thereby increasing the barrier and preventing a high pressure metastable state from returning to the initial stable state after the pressure is released (Figure 8b). After that, Zou and coworkers[121] selected the organic molecule 4-aminopyridinium (4AMP) with complex configuration to prepare and study the high-pressure behavior of 0D organic-inorganic hybrid perovskite $(4AMP)_2ZnBr_4$ (AMP = $C_5H_7N_2$). The pressure treatment adjusted the "sky blue light" before compression to "cool daylight" (Figure 8c), with a remarkable quantum yield of 88.52% after decompression, which was 10 times that under ambient conditions. As expected, high-efficiency emission was maintained under environmental

DOI: 10.31635/ccschem.024.202405293
Citation: *CCS Chem.* **2025**, 7, 1250–1271
Link to VoR: https://doi.org/10.31635/ccschem.024.202405293

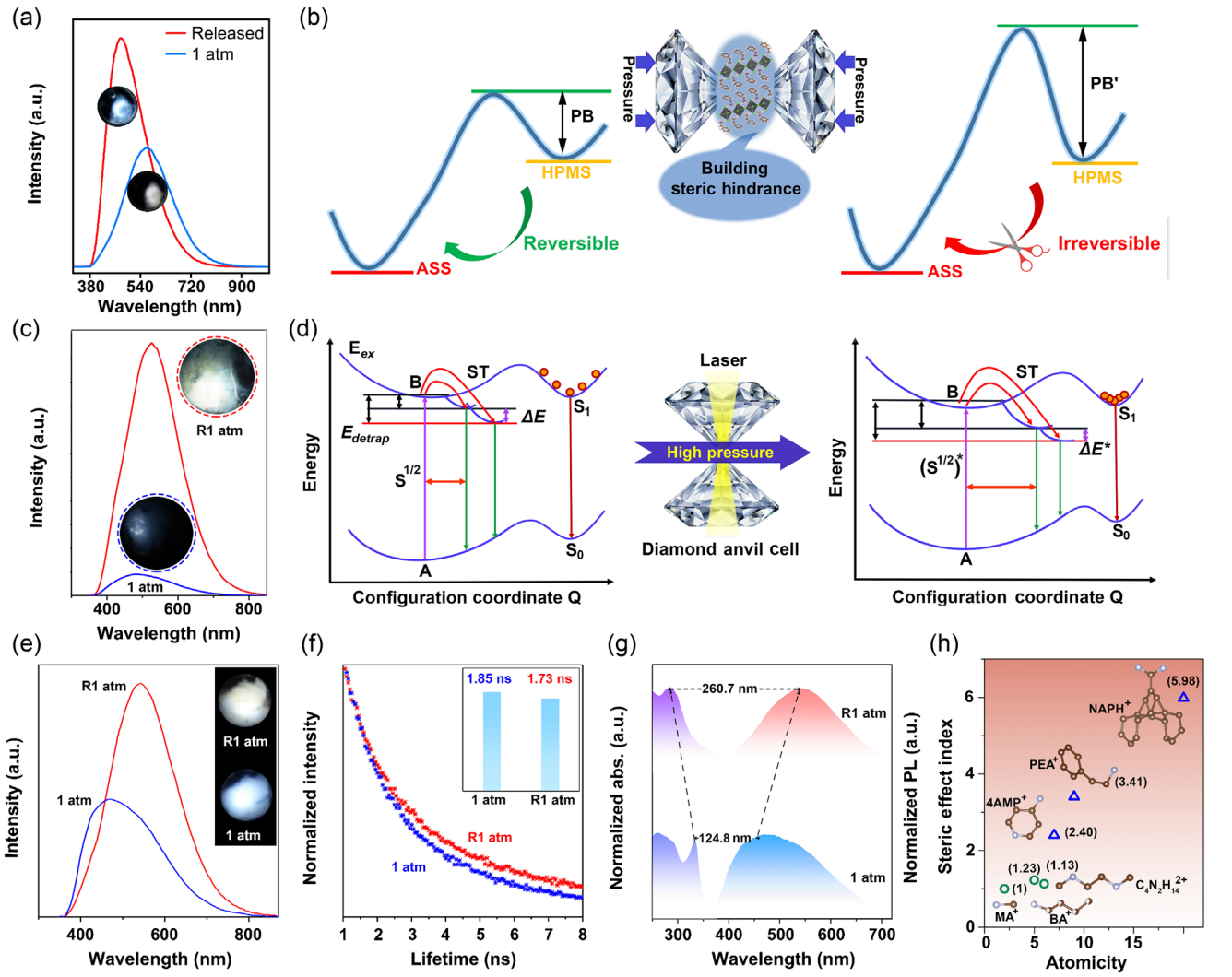

Figure 8 | *(a) Comparison of emission spectra for $(PEA)_2PbCl_4$ NCs before and after pressure treatment. Reprinted with permission from ref 120. Copyright 2021 Wiley-VCH. (b) Illustrated mechanism of the retention of PIE associated with steric hindrance of complex compact organic molecules. Reprinted with permission from ref 120. Copyright 2021 Wiley-VCH. (c) Comparison of emission spectra for $(4AMP)_2ZnBr_4$ MTs before and after pressure treatment. Reprinted with permission from ref 121. Copyright 2021 Wiley-VCH. (d) Configuration coordinate models at 1 atm and high pressure. Reprinted with permission from ref 121. Copyright 2021 Wiley-VCH. (e) Comparison of emission spectra of $(NAPH)_2PbCl_4$ NPs before and after pressure treatment. Inset shows the corresponding photographs. Reprinted with permission from ref 122. Copyright 2023 Cell Press. (f) Lifetime comparison of white-light emission in $(NAPH)_2PbCl_4$ before and after pressure treatment. Reprinted with permission from ref 122. Copyright 2023 Cell Press. (g) Stokes shift comparison of white-light emission in $(NAPH)_2PbCl_4$ before and after pressure treatment. Reprinted with permission from ref 122. Copyright 2023 Cell Press. (h) Calculation of SEI induced by MA^+, BA^+, $C_4N_2H_{14}^{2+}$, 4-AMP^+, PEA^+, and $NAPH^+$, respectively. Reprinted with permission from ref 122. Copyright 2023 Cell Press.*

conditions. Under high pressure, the distorted 4AMP molecular motifs led to the charge being more localized, and the electron-phonon coupling and quantum confinement effects were also enhanced, thus promoting the radiative recombination of the emission of singlet excitons (Figure 8d). Therefore, the irreversible electronic structural transition induced by steric hindrance is an important reason for the final retention of PIE and tuning of the color temperature.

The idea of steric hindrance undoubtedly provides a new way for the preservation of high-pressure phase. Nonetheless, quantitative determination of the steric hindrance effect on the eventual retention of PIE remains elusive and a great challenge. Start with the high-pressure study of naphthyl perovskites, Zhao et al.[122] quantitatively evaluated the steric hindrance of multiple organic molecules and defined the steric effect index (SEI). Naphthyl perovskite $(NAPH)_2PbCl_4$ (NAPH = 1-(2-naphthyl)methanamine) after

DOI: 10.31635/ccschem.024.202405293
Citation: *CCS Chem.* **2025**, 7, 1250–1271
Link to VoR: https://doi.org/10.31635/ccschem.024.202405293

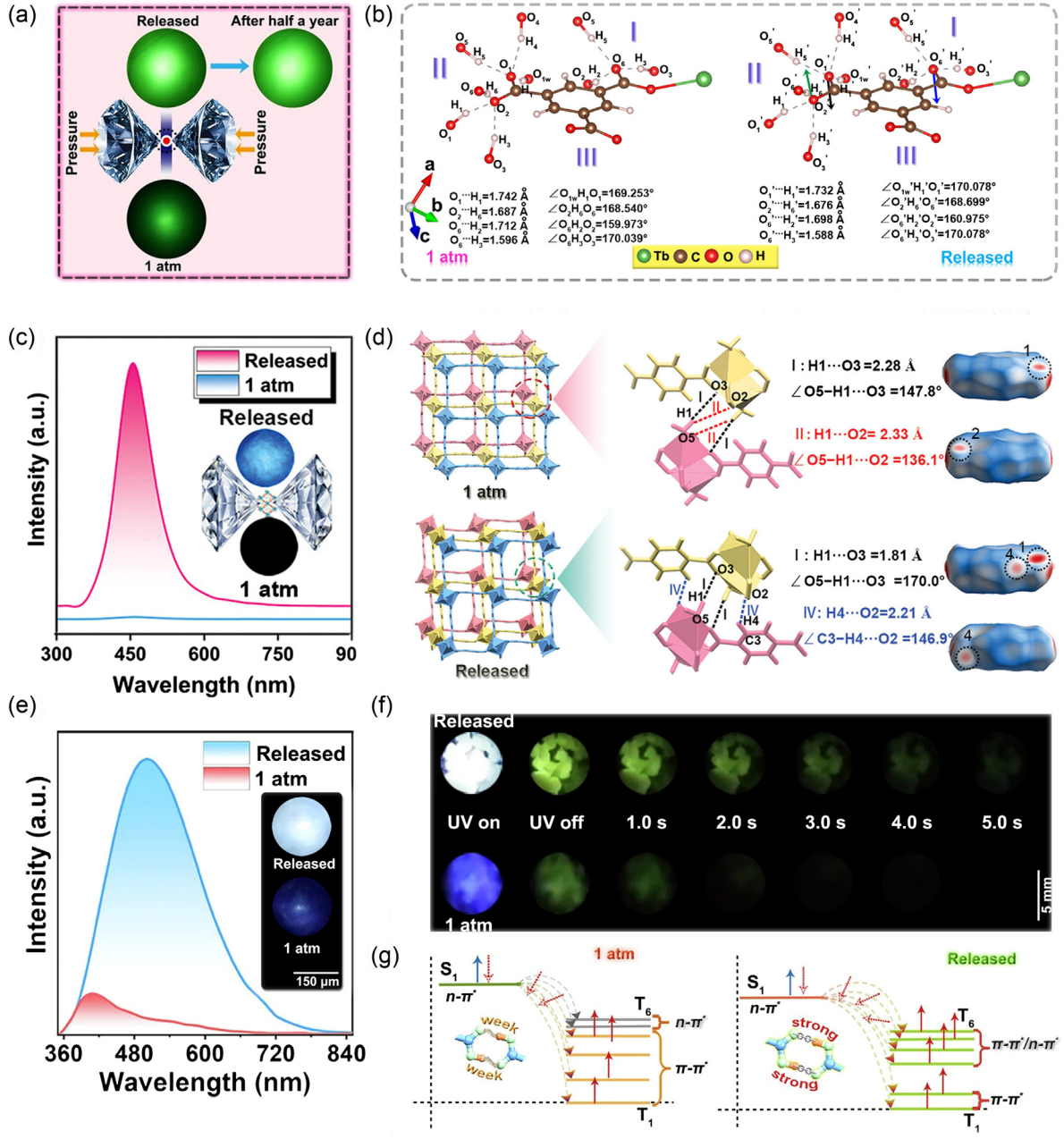

Figure 9 | *(a) Comparison of PL micrographs for Tb(BTC)(H$_2$O)$_6$ before and after pressure treatment. Reprinted with permission from ref 123. Copyright 2022 Wiley-VCH GmbH. (b) Comparison of hydrogen bonds between H and O for Tb(BTC)(H$_2$O)$_6$ before and after pressure treatment. Reprinted with permission from ref 123. Copyright 2022 Wiley-VCH GmbH. (c) PL spectra and corresponding PL photographs of MOF-2 before and after pressure treatment. Reprinted with permission from ref 125. Copyright 2023 Wiley-VCH GmbH. (d) Hydrogen bonding interactions of MOF-2 before and after pressure treatment. Reprinted with permission from ref 125. Copyright 2023 Wiley-VCH GmbH. (e) PL spectra and corresponding PL photographs of IPA before and after pressure treatment. Reprinted with permission from ref 126. Copyright 2024 Nature Publishing Group. (f) Photographs of the pristine and pressure-treated IPA taken at different time intervals before and after turning off the laser excitation (355 nm) at ambient conditions. Reprinted with permission from ref 126. Copyright 2024 Nature Publishing Group. (g) Schematic representation of strengthened hydrogen bonds acting after pressure treatment, promoting the mixture of $^3(\pi, \pi^*)$ and $^3(n, \pi^*)$ transitions, thus accelerating the ISC process. Reprinted with permission from ref 126. Copyright 2024 Nature Publishing Group.*

DOI: 10.31635/ccschem.024.202405293
Citation: *CCS Chem.* **2025**, 7, 1250–1271
Link to VoR: https://doi.org/10.31635/ccschem.024.202405293

pressure treatment successfully obtained amorphous states with high-efficiency warm white light, reduced decay time, and extended Stokes shift (Figure 8e–g). Given this, the SEI value of NAPH was calculated to be 5.98, which is the highest SEI compared to other molecules (Figure 8h). Accordingly, the high steric hindrance of organic $NAPH^+$ cations with complex configurations increased the barrier of phase transition, which was responsible for the ultimate pressure-induced irreversibility. Thus, the correlation between PIE retention and steric hindrance has been successfully established, providing a promising strategy for rational structural design of high-performance materials.

High-pressure phase retention: hydrogen bonding cooperativity effect

Apart from using nanosize effects and steric hindrance effects to improve steric hindrance, Zou and coworkers[123] innovatively proposed a new strategy for hydrogen bonding cooperativity to stabilize high-pressure phases. Based on the hypothesis that lanthanide metal organic frameworks (Ln-MOFs) are expected to realize ligand-to-metal energy transfer (LMET) by means of high-pressure regulation of hydrogen bond enhancement in ligand, high pressure studies were carried out on Tb(BTC)$(H_2O)_6$ containing hydrogen bonding.[123] As predicted, Tb(BTC)$(H_2O)_6$ exhibited bright green light emission after pressure treatment and the photoluminescence quantum yield increased from 50.6% to 90.4% (Figure 9a). The high-pressure experiments and theoretical calculations finally determined the reason for the enhanced green emission after pressure relief: the enhanced hydrogen bonds successfully locked the conjugated configuration formed by the two planes of carboxylic acid group and benzene ring in the ligand, which promoted the intersystem crossing (ISC) process (Figure 9b). Moreover, the optimized singlet and triplet states also validated the facilitated LMET process, acquiring the green photoluminescence (PL) enhancement of MOFs under the aforementioned two collaboration effects. Subsequently, the same strategy was applied to Y(BTC)$(H_2O)_6$, achieving the interception of bright blue light.[124] Compared with pressure-regulated PL enhancement, PL turn-on behavior in nonemissive materials is more challenging. Yang et al.[125] reported initial nonemissive Zn(BDC)(DMF)(H_2O) (MOF-2) (BDC = 1, 4-benzenedicarboxylate and DMF = *N*, *n*-dimethylformamide) switched on bright blue emission after pressure treatment (Figure 9c). With the help of the pressure treatment engineering, the hydrogen-bonding cooperativity effect powerfully increased the rotation barrier of the phenyl group from the initial 0.91 to 3.87 eV mol^{-1} (Figure 9d). The apparent limitation of rotation and vibration-reduced nonradiative losses facilitated the radiative transition process and triggered a bright blue light under ambient conditions. Pressure treatment engineering has great potential not only for precise regulation of fluorescence, but also for efficient optimization of phosphorescence. Luminous materials containing both bright singlet and triplet excitons play an indispensable role in the field of optoelectronics applications. However, the imbalanced contribution of fluorescence and phosphorescence inherent in luminous materials seriously hinders the realization of high-performance white light emission. More recently, Zou and coworkers[126] applied pressure treatment engineering to isophthalic acid (IPA), a material that emits a mixture of fluorescence and phosphorescence. Happily, the balance of fluorescence and phosphorescence emission in IPA was reconstructed, yielding high-performance white emission with chromaticity coordinates of (0.28, 0.36) (Figure 9e,f). The pressure treatment engineering tremendously boosted the mixture of $n–\pi^*/\pi–\pi^*$ transition configurations in targeted triplet states by strengthening hydrogen bonds, which triggered an enhancement of spin-orbital coupling (SOC) favoring efficient ISC (Figure 9g). Meanwhile, the nonradiative dissipation of singlet and triplet excitons are substantially suppressed by the enhanced hydrogen bonds, empowering the treated IPA to carry distinguishable higher fluorescent and phosphorescent efficiency.

To this end, the above three strategies for enhancing phase transition barriers have been successfully developed. The stabilization of the high-pressure phase and the preservation of novel properties provide a promising strategy for developments in lighting, sensing, display, and other fields.

Conclusion, Outlook and Challenge

Chemical synthesis driven by high pressure is an important direction of high-pressure chemistry. In this review, the synthesis of organic and inorganic materials under high pressure and the retention of the high-pressure phase with better properties were summarized. The underlying mechanism of synthesis and retention was further discussed. This review is believed to provide guidance for designing high-performance materials by expanding the paths of chemical synthesis, thus greatly exploiting the existing materials world with newly emerging and enhanced functionalities. So far, the synthesis and analysis of organic compounds under high pressure, from small molecules to more complex organic compounds, have been achieved. Moreover, a significant number of inorganic compounds, including but not limited to hydrides, borides, carbides, nitrides, chalcogenides, halides, and alloys, have also been prepared by multianvil presses or diamond anvil cell devices. In addition, the retention of high-pressure phases with better properties is another milestone achievement after PIE. Strategies such as nanosize effect, steric hindrance

DOI: 10.31635/ccschem.024.202405293
Citation: *CCS Chem.* **2025**, 7, 1250–1271
Link to VoR: https://doi.org/10.31635/ccschem.024.202405293

effect, and the hydrogen bonding cooperativity effect have been explored to preserve the high-pressure phase. Moreover, the retention of high-performance, high-pressure phases enables the large-scale preparation by employing the large volume press. The discovery of new phases of materials and the synthesis of new substances will greatly deepen people's understanding of materials. High-pressure phase harvesting would be promising candidates for practical applications in the fields of solid-state lighting, display, sensing, anti-counterfeiting, information encryption, and so on. These breakthroughs have made outstanding contributions to the exploration of new materials and the discovery of new properties. There is no doubt that high-pressure synthesis and the retention of high-pressure phases will continue to provide more research innovations of scientific significance in the future.

Although great success has been achieved in the field of high-pressure chemistry, some new issues remain challenging to overcome. The precise atomic-scale synthesis of high-pressure products and the functionalization exploration of high-quality products are the core challenges in the future development of high-pressure organic synthesis. To this end, more systematic high-pressure synthesis strategies and design schemes of precursor molecule need to be explored. In addition, the mechanism of organic synthesis under high pressure still remains elusive. Meanwhile, restrictive factors, such as expensive experimental costs, complex high-pressure equipment to operate, and low accuracy between theoretical prediction and high-pressure material characterization techniques, all delay the development of new inorganic materials. Future research should focus on simplifying high-pressure equipment, developing diverse in situ characterization techniques, and improving precision of theoretical predictions under high-pressure conditions including machine learning to accelerate high-pressure synthesis of novel inorganic materials. For the high-pressure phase retention after structural phase transition, most quenched phases are disordered amorphous states, which are difficult to be identified accurately by the limited micro-characterizations. The development of in situ high-pressure instruments and techniques is an urgent requirement, including vibrational spectroscopy, neutron scattering and pair distribution function, and so on. Likewise, more effective ways to capture high-pressure phases may be developed by introducing additional dimensions, such as low temperature, shear force, and rate of rise and fall of pressure. Furthermore, some quenched metastable phases or superior properties required much higher pressure treatment in order to be stabilized at ambient conditions. This will bring great challenges to large-scale synthesis. The breakthrough of pressure loading limits of large volume presses are therefore urgently demanded. We firmly believe that the information provided in this mini-review will not only provide more research opportunities that are important for developing high-pressure chemistry, but also be expected to broaden horizons and expand interdisciplinary ideas for chemistry in the future.

Acknowledgments

This work is supported by the National Key R&D Program of China (grant nos. 2022YFA1402300, 2023YFA1406200, and 2019YFA0708502) and the National Science Foundation of China (grant nos. 22131006, 12174144, 12474009, 22022101, and 22090041).

References

1. Xiao, G.; Geng, T.; Zou, B. Emerging Functional Materials Under High Pressure Toward Enhanced Properties. *ACS Mater. Lett.* **2020**, *2*, 1233–1239.
2. Zhao, W.; Xiao, G.; Zou, B. Pressure-Induced Emission (PIE) in Halide Perovskites Toward Promising Applications in Scintillators and Solid-State Lighting. *Aggregate* **2024**, *5*, e461.
3. Cho, E. S.; Coates, N. E.; Forster, J. D.; Ruminski, A. M.; Russ, B.; Sahu, A.; Su, N. C.; Yang, F.; Urban, J. J. Engineering Synergy: Energy and Mass Transport in Hybrid Nanomaterials. *Adv. Mater.* **2015**, *27*, 5744–5752.
4. Ming, H.; Luo, Z. Z.; Chen, Z.; Cui, H. H.; Zheng, W.; Zou, Z.; Kanatzidis, M. G. Chemical Pressure-Driven Band Convergence and Discordant Atoms Intensify Phonon Scattering Leading to High Thermoelectric Performance in SnTe. *J. Am. Chem. Soc.* **2024**, *146*, 28448–28458.
5. Zhang, T.; Yu, S.; Wu, Y.; Ibrahim, M. A.; Walter, A. D.; Schwenk, G. R.; Hu, Y. J.; Barsoum, M. W.; Li, C. Y. Tuning the 1D-to-2D Transition in Lepidocrocite Titanate Nanofilaments via Polymer Wrapping. *Matter* **2024**, *7*, 3422–3432.
6. Ma, Z.; Li, F.; Sui, L.; Shi, Y.; Fu, R.; Yuan, K.; Xiao, G.; Zou, B. Tunable Color Temperatures and Emission Enhancement in 1d Halide Perovskites Under High Pressure. *Adv. Opt. Mater.* **2020**, *8*, 2000713.
7. Wang, Y.; Guo, S.; Luo, H.; Zhou, C.; Lin, H.; Ma, X.; Hu, Q.; Du, M. H.; Ma, B.; Yang, W.; Lü, X. Reaching 90% Photoluminescence Quantum Yield in One-Dimensional Metal Halide $C_4N_2H_{14}PbBr_4$ by Pressure-Suppressed Nonradiative Loss. *J. Am. Chem. Soc.* **2020**, *142*, 16001–16006.
8. Xiao, G.; Cao, Y.; Qi, G.; Wang, L.; Liu, C.; Ma, Z.; Yang, X.; Sui, Y.; Zheng, W.; Zou, B. Pressure Effects on Structure and Optical Properties in Cesium Lead Bromide Perovskite Nanocrystals. *J. Am. Chem. Soc.* **2017**, *139*, 10087–10094.
9. Margetic, D. *High Pressure Organic Synthesis*; De Gruyter: Berlin, Boston, **2019**.
10. Wang, Y.; Yang, X.; Tang, X.; Wang, X.; Li, Y.; Lin, X.; Dong, X.; Yang, D.; Zheng, H.; Li, K.; Mao, H. K. Pressure Gradient Squeezing Hydrogen Out of MnOOH: Thermodynamics and Electrochemistry. *J. Phys. Chem. Lett.* **2021**, *12*, 10893–10898.

DOI: 10.31635/ccschem.024.202405293
Citation: *CCS Chem.* **2025**, 7, 1250–1271
Link to VoR: https://doi.org/10.31635/ccschem.024.202405293

11. Wang, Y.; Che, G.; Yang, X.; Zheng, J.; Lin, Y.; Zheng, H.; Li, K.; Mao, H. K. Piezovoltaics from PdH_x. *J. Phys. Chem. Lett.* **2023**, *14*, 3168–3173.
12. Chen, B.; Hoffmann, R.; Cammi, R. The Effect of Pressure on Organic Reactions in Fluids—A New Theoretical Perspective. *Angew. Chem. Int. Ed.* **2017**, *56*, 11126–11142.
13. Zerr, A.; Serghiou, G.; Boehler, R.; Ross, M. Decomposition of Alkanes at High Pressures and Temperatures. *High Press. Res.* **2006**, *26*, 23–32.
14. Wieldraaijer, H. H.; Schouten, J. A.; Trappeniers, N. J. Investigation of the Phase Diagrams of Ethane, Ethylene, and Methane at High Pressures. *High Temp.-High Press.* **1983**, *15*, 87–92.
15. Chelazzi, D.; Ceppatelli, M.; Santoro, M.; Bini, R.; Schettino, V. Pressure-Induced Polymerization in Solid Ethylene. *J. Phys. Chem. B* **2005**, *109*, 21658–21663.
16. Aoki, K.; Usuba, S.; Yoshida, M.; Kakudate, Y.; Tanaka, K.; Fujiwara, S. Raman Study of the Solid-State Polymerization of Acetylene at High Pressure. *J. Chem. Phys.* **1988**, *89*, 529–534.
17. Trout, C. C.; Badding, J. V. Solid State Polymerization of Acetylene at High Pressure and Low Temperature. *J. Phys. Chem. A* **2000**, *104*, 8142–8145.
18. Gou, H.; Zhu, L.; Huang, H.-T.; Biswas, A.; Keefer, D. W.; Chaloux, B. L.; Prescher, C.; Yang, L.; Kim, D. Y.; Ward, M. D.; Lerach, J.; Wang, S.; Oganov, A. R.; Epshteyn, A.; Badding, J. V.; Strobel, T. A. From Linear Molecular Chains to Extended Polycyclic Networks: Polymerization of Dicyanoacetylene. *Chem. Mater.* **2017**, *29*, 6706–6718.
19. Ward, M. D.; Huang, H. T.; Zhu, L.; Popov, D.; Strobel, T. A. High-Pressure Behavior of C_2I_2 and Polymerization to a Conductive Polymer. *J. Phys. Chem. C* **2019**, *123*, 11369–11377.
20. Wang, X.; Tang, X.; Zhang, P.; Wang, Y.; Gao, D.; Liu, J.; Hui, K.; Wang, Y.; Dong, X.; Hattori, T.; Sano-Furukawa, A.; Ikeda, K.; Miao, P.; Lin, X.; Tang, M.; Zuo, Z.; Zheng, H.; Li, K.; Mao, H. K. Crystalline Fully Carboxylated Polyacetylene Obtained Under High Pressure as a Li-Ion Battery Anode Material. *J. Phys. Chem. Lett.* **2021**, *12*, 12055–12061.
21. Zheng, H.; Li, K.; Cody, G. D.; Tulk, C. A.; Dong, X.; Gao, G.; Molaison, J. J.; Liu, Z.; Feygenson, M.; Yang, W.; Ivanov, I. N.; Basile, L.; Idrobo, J. C.; Guthrie, M.; Mao, H. K. Polymerization of Acetonitrile via a Hydrogen Transfer Reaction from CH_3 to CN Under Extreme Conditions. *Angew. Chem. Int. Ed.* **2016**, *55*, 12040–12044.
22. Zhang, P.; Tang, X.; Zhang, C.; Gao, D.; Wang, X.; Wang, Y.; Guo, W.; Zou, R.; Han, Y.; Lin, X.; Dong, X.; Li, K.; Zheng, H.; Mao, H. K. Pressure-Induced Hydrogen Transfer in 2-Butyne via a Double CH$\cdots\pi$ Aromatic Transition State. *J. Phys. Chem. Lett.* **2022**, *13*, 4170–4175.
23. Stojkovic, D.; Zhang, P.; Crespi, V. H. Smallest Nanotube: Breaking the Symmetry of sp^3 Bonds in Tubular Geometries. *Phys. Rev. Lett.* **2001**, *87*, 125502.
24. Xu, E. S.; Lammert, P. E.; Crespi, V. H. Systematic Enumeration of sp^3 Nanothreads. *Nano Lett.* **2015**, *15*, 5124–5130.
25. Fitzgibbons, T. C.; Guthrie, M.; Xu, E. S.; Crespi, V. H.; Davidowski, S. K.; Cody, G. D.; Alem, N.; Badding, J. V. Benzene-Derived Carbon Nanothreads. *Nat. Mater.* **2014**, *14*, 43–47.
26. Li, X.; Baldini, M.; Wang, T.; Chen, B.; Xu, E. S.; Vermilyea, B.; Crespi, V. H.; Hoffmann, R.; Molaison, J. J.; Tulk, C. A.; Guthrie, M.; Sinogeikin, S.; Badding, J. V. Mechanochemical Synthesis of Carbon Nanothread Single Crystals. *J. Am. Chem. Soc.* **2017**, *139*, 16343–16349.
27. Duan, P.; Li, X.; Wang, T.; Chen, B.; Juhl, S. J.; Koeplinger, D.; Crespi, V. H.; Badding, J. V.; Schmidt-Rohr, K. The Chemical Structure of Carbon Nanothreads Analyzed by Advanced Solid-State NMR. *J. Am. Chem. Soc.* **2018**, *140*, 7658–7666.
28. Chen, B.; Hoffmann, R.; Ashcroft, N.; Badding, J.; Xu, E.; Crespi, V. Linearly Polymerized Benzene Arrays as Intermediates, Tracing Pathways to Carbon Nanothreads. *J. Am. Chem. Soc.* **2015**, *137*, 14373–14386.
29. Juhl, S. J.; Wang, T.; Vermilyea, B.; Li, X.; Crespi, V. H.; Badding, J. V.; Alem, N. Local Structure and Bonding of Carbon Nanothreads Probed by High-Resolution Transmission Electron Microscopy. *J. Am. Chem. Soc.* **2019**, *141*, 6937–6945.
30. Gao, D.; Tang, X.; Wang, X.; Yang, X.; Zhang, P.; Che, G.; Han, J.; Hattori, T.; Wang, Y.; Dong, X.; Zheng, H.; Li, K.; Mao, H. K. Phase Transition and Chemical Reactivity of 1H-Tetrazole Under High Pressure Up to 100 GPa. *Phys. Chem. Chem. Phys.* **2021**, *23*, 19503–19510.
31. Huss, S.; Wu, S.; Chen, B.; Wang, T.; Gerthoffer, M. C.; Ryan, D. J.; Smith, S. E.; Crespi, V. H.; Badding, J. V.; Elacqua, E. Scalable Synthesis of Crystalline One-Dimensional Carbon Nanothreads Through Modest-Pressure Polymerization of Furan. *ACS Nano* **2021**, *15*, 4134–4143.
32. Biswas, A.; Ward, M. D.; Wang, T.; Zhu, L.; Huang, H. T.; Badding, J. V.; Crespi, V. H.; Strobel, T. A. Evidence for Orientational Order in Nanothreads Derived from Thiophene. *J. Phys. Chem. Lett.* **2019**, *10*, 7164–7171.
33. Wang, K.; Liu, J.; Yang, K.; Liu, B.; Zou, B. High-Pressure-Induced Polymorphic Transformation of Maleic Hydrazide. *J. Phys. Chem. C* **2014**, *118*, 8122–8127.
34. Dunning, S. G.; Zhu, L.; Chen, B.; Chariton, S.; Prakapenka, V. B.; Somayazulu, M.; Strobel, T. A. Solid-State Pathway Control via Reaction-Directing Heteroatoms: Ordered Pyridazine Nanothreads Through Selective Cycloaddition. *J. Am. Chem. Soc.* **2022**, *144*, 2073–2078.
35. Gao, D.; Tang, X.; Xu, J.; Yang, X.; Zhang, P.; Che, G.; Wang, Y.; Chen, Y.; Gao, X.; Dong, X.; Zheng, H.; Li, K.; Mao, H. K. Crystalline $C_3N_3H_3$ Tube (3,0) Nanothreads. *Proc. Natl. Acad. Sci. U.S.A.* **2022**, *119*, e2201165119.
36. Friedrich, A.; Collings, I. E.; Dziubek, K. F.; Fanetti, S.; Radacki, K.; Ruiz-Fuertes, J.; Pellicer-Porres, J.; Hanfland, M.; Sieh, D.; Bini, R.; Clark, S. J.; Marder, T. B. Pressure-Induced Polymerization of Polycyclic Arene-Perfluoroarene Cocrystals: Single Crystal X-Ray Diffraction Studies, Reaction Kinetics, and Design of Columnar Hydrofluorocarbons. *J. Am. Chem. Soc.* **2020**, *142*, 18907–18923.
37. Ward, M. D.; Tang, W. S.; Zhu, L.; Popov, D.; Cody, G. D.; Strobel, T. A. Controlled Single-Crystalline Polymerization of $C_{10}H_8 \cdot C_{10}F_8$ Under Pressure. *Macromolecules* **2019**, *52*, 7557–7563.
38. Wang, X.; Yang, X.; Wang, Y.; Tang, X.; Zheng, H.; Zhang, P.; Gao, D.; Che, G.; Wang, Z.; Guan, A.; Xiang, J. F.; Tang, M.; Dong, X.; Li, K.; Mao, H. K. From Biomass to Functional

DOI: 10.31635/ccschem.024.202405293
Citation: *CCS Chem.* **2025**, 7, 1250–1271
Link to VoR: https://doi.org/10.31635/ccschem.024.202405293

Crystalline Diamond Nanothread: Pressure-Induced Polymerization of 2,5-Furandicarboxylic Acid. *J. Am. Chem. Soc.* **2022**, *144*, 21837–21842.
39. Dunning, S. G.; Chen, B.; Zhu, L.; Cody, G. D.; Chariton, S.; Prakapenka, V. B.; Zhang, D.; Strobel, T. A. Synthesis and Post-Processing of Chemically Homogeneous Nanothreads from 2,5-Furandicarboxylic Acid. *Angew. Chem. Int. Ed.* **2023**, *62*, e202217023.
40. Oburn, S. M.; Huss, S.; Cox, J.; Gerthoffer, M. C.; Wu, S.; Biswas, A.; Murphy, M.; Crespi, V. H.; Badding, J. V.; Lopez, S. A.; Elacqua, E. Photochemically Mediated Polymerization of Molecular Furan and Pyridine: Synthesis of Nanothreads at Reduced Pressures. *J. Am. Chem. Soc.* **2022**, *144*, 22026–22034.
41. Zhang, P.; Tang, X.; Wang, Y.; Wang, X.; Gao, D.; Li, Y.; Zheng, H.; Wang, Y.; Wang, X.; Fu, R.; Tang, M.; Ikeda, K.; Miao, P.; Hattori, T.; Sano-Furukawa, A.; Tulk, C. A.; Molaison, J. J.; Dong, X.; Li, K.; Ju, J.; Mao, H. K. Distance-Selected Topochemical Dehydro-Diels-Alder Reaction of 1,4-Diphenylbutadiyne Toward Crystalline Graphitic Nanoribbons. *J. Am. Chem. Soc.* **2020**, *142*, 17662–17669.
42. Li, Y.; Tang, X.; Zhang, P.; Wang, Y.; Yang, X.; Wang, X.; Li, K.; Wang, Y.; Wu, N.; Tang, M.; Xiang, J.; Lin, X.; Lee, H. H.; Dong, X.; Zheng, H.; Mao, H. K. Scalable High-Pressure Synthesis of sp^2-sp^3 Carbon Nanoribbon via [4+2] Polymerization of 1,3,5-Triethynylbenzene. *J. Phys. Chem. Lett.* **2021**, *12*, 7140–7145.
43. Zhang, P.; Gao, D.; Tang, X.; Yang, X.; Zheng, H.; Wang, Y.; Wang, X.; Xu, J.; Wang, Z.; Liu, J.; Wang, X.; Ju, J.; Tang, M.; Dong, X.; Li, K.; Mao, H. K. Ordered Van Der Waals Heterо-Nanoribbon from Pressure-Induced Topochemical Polymerization of Azobenzene. *J. Am. Chem. Soc.* **2023**, *145*, 6845–6852.
44. Sun, J.; Dong, X.; Wang, Y.; Li, K.; Zheng, H.; Wang, L.; Cody, G. D.; Tulk, C. A.; Molaison, J. J.; Lin, X.; Meng, Y.; Jin, C.; Mao, H. K. Pressure-Induced Polymerization of Acetylene: Structure-Directed Stereoselectivity and a Possible Route to Graphane. *Angew. Chem. Int. Ed.* **2017**, *56*, 6553–6557.
45. Wang, Y.; Dong, X.; Tang, X.; Zheng, H.; Li, K.; Lin, X.; Fang, L.; Sun, G. A.; Chen, X.; Xie, L.; Bull, C. L.; Funnell, N. P.; Hattori, T.; Sano-Furukawa, A.; Chen, J.; Hensley, D. K.; Cody, G. D.; Ren, Y.; Lee, H. H.; Mao, H. K. Pressure-Induced Diels-Alder Reactions in C_6H_6-C_6F_6 Cocrystal Towards Graphane Structure. *Angew. Chem. Int. Ed.* **2019**, *58*, 1468–1473.
46. Huang, H. T.; Zhu, L.; Ward, M. D.; Wang, T.; Chen, B.; Chaloux, B. L.; Wang, Q.; Biswas, A.; Gray, J. L.; Kuei, B.; Cody, G. D.; Epshteyn, A.; Crespi, V. H.; Badding, J. V.; Strobel, T. A. Nanoarchitecture Through Strained Molecules: Cubane-Derived Scaffolds and the Smallest Carbon Nanothreads. *J. Am. Chem. Soc.* **2020**, *142*, 17944–17955.
47. Yang, X.; Che, G.; Li, F.; Tang, X.; Wang, Y.; Wang, Y.; Guan, A.; Xiang, J.; Li, Q.; Liu, J.; Dong, X.; Mao, H. K.; Zheng, H.; Li, K. Fused-Ring Carbon Nanothread Synthesized by Pressure-Induced Polymerization of Azulene. *J. Phys. Chem. C.* **2024**, *128*, 16011–16019.
48. Fei, Y.; Li, Y.; Lang, P.; Tang, X.; Zhang, P.; Che, G.; Dong, X.; Li, K.; Zheng, H. High Pressure Polymerization of 2,6-Diethynylpyridine. *J. Phys. Chem. C* **2024**, *128*, 7286–7293.
49. Ciabini, L.; Santoro, M.; Gorelli, F. A.; Bini, R.; Schettino, V.; Raugei, S. Triggering Dynamics of the High-Pressure Benzene Amorphization. *Nat. Mater.* **2006**, *6*, 39–43.
50. Tang, X.; Dong, X.; Zhang, C.; Li, K.; Zheng, H.; Mao, H. K. Triggering Dynamics of Acetylene Topochemical Polymerization. *Matter Radiat. Extremes* **2023**, *8*, 058402.
51. Huppertz, H.; Heymann, G.; Schwarz, U.; Schwarz, M. R. High-Pressure Methods in Solid-State Chemistry. In *Handbook of Solid State Chemistry*; **2017**; pp 23–48.
52. Inaguma, Y. High-Pressure Perovskite: Synthesis, Structure, and Phase Relation. In *Handbook of Solid State Chemistry*; **2017**; pp 49–106.
53. Zhu, C.; Yang, J.; Shan, P.; Zhao, M. H.; Zhao, S.; Pei, C.; Zhang, B.; Deng, Z.; Croft, M.; Qi, Y.; Yang, L.; Wang, Y.; Kuang, X.; Jiang, L.; Yao, D. X.; Cheng, J. G.; Li, M. R. Pressure-Induced Intermetallic Charge Transfer and Semiconductor-Metal Transition in Two-Dimensional $AgRuO_3$. *CCS Chem.* **2022**, *5*, 934–946.
54. Sun, H.; Huo, M.; Hu, X.; Li, J.; Liu, Z.; Han, Y.; Tang, L.; Mao, Z.; Yang, P.; Wang, B.; Cheng, J.; Yao, D. X.; Zhang, G. M.; Wang, M. Signatures of Superconductivity Near 80 K in a Nickelate Under High Pressure. *Nature* **2023**, *621*, 493–498.
55. Belik, A. A.; Yi, W. High-Pressure Synthesis, Crystal Chemistry and Physics of Perovskites with Small Cations at the a Site. *J. Phys.: Condens. Mat.* **2014**, *26*, 163201.
56. Li, M. R.; Croft, M.; Stephens, P. W.; Ye, M.; Vanderbilt, D.; Retuerto, M.; Deng, Z.; Grams, C. P.; Hemberger, J.; Hadermann, J.; Li, W. M.; Jin, C. Q.; Saouma, F. O.; Jang, J. I.; Akamatsu, H.; Gopalan, V.; Walker, D.; Greenblatt, M. Mn_2FeWO_6: A New Ni_3TeO_6-Type Polar and Magnetic Oxide. *Adv. Mater.* **2015**, *27*, 2177–2181.
57. Li, M. R.; McCabe, E. E.; Stephens, P. W.; Croft, M.; Collins, L.; Kalinin, S. V.; Deng, Z.; Retuerto, M.; Sen Gupta, A.; Padmanabhan, H.; Gopalan, V.; Grams, C. P.; Hemberger, J.; Orlandi, F.; Manuel, P.; Li, W. M.; Jin, C. Q.; Walker, D.; Greenblatt, M. Magnetostriction-Polarization Coupling in Multiferroic Mn_2MnWO_6. *Nat. Commun.* **2017**, *8*, 2037.
58. Li, M. R.; Retuerto, M.; Deng, Z.; Stephens, P. W.; Croft, M.; Huang, Q.; Wu, H.; Deng, X.; Kotliar, G.; Sanchez-Benitez, J.; Hadermann, J.; Walker, D.; Greenblatt, M. Giant Magnetoresistance in the Half-Metallic Double-Perovskite Ferrimagnet Mn_2FeReO_6. *Angew. Chem. Int. Ed.* **2015**, *54*, 12069–12073.
59. Arévalo-López, A. M.; McNally, G. M.; Attfield, J. P. Large Magnetization and Frustration Switching of Magnetoresistance in the Double-Perovskite Ferrimagnet Mn_2FeReO_6. *Angew. Chem. Int. Ed.* **2015**, *54*, 12074–12077.
60. Zhou, L.; Dai, J.; Chai, Y.; Zhang, H.; Dong, S.; Cao, H.; Calder, S.; Yin, Y.; Wang, X.; Shen, X.; Liu, Z.; Saito, T.; Shimakawa, Y.; Hojo, H.; Ikuhara, Y.; Azuma, M.; Hu, Z.; Sun, Y.; Jin, C.; Long, Y. Realization of Large Electric Polarization and Strong Magnetoelectric Coupling in $BiMn_3Cr_4O_{12}$. *Adv. Mater.* **2017**, *29*, 1703435.
61. Liu, Z.; Zhang, S.; Wang, X.; Ye, X.; Qin, S.; Shen, X.; Lu, D.; Dai, J.; Cao, Y.; Chen, K.; Radu, F.; Wu, W. B.; Chen, C. T.; Francoual, S.; Mardegan, J. R. L.; Leupold, O.; Tjeng, L. H.; Hu, Z.; Yang, Y. F.; Long, Y. Realization of a Half Metal with a

DOI: 10.31635/ccschem.024.202405293
Citation: *CCS Chem.* **2025**, 7, 1250–1271
Link to VoR: https://doi.org/10.31635/ccschem.024.202405293

Record-High Curie Temperature in Perovskite Oxides. *Adv. Mater.* **2022**, *34*, e2200626.
62. Yue, B.; Zhong, W.; Deng, W.; Wen, T.; Wang, Y.; Yin, Y.; Shan, P.; Wang, J. T.; Yu, X.; Hong, F. Insulator-to-Superconductor Transition in Quasi-One-Dimensional HfS_3 Under Pressure. *J. Am. Chem. Soc.* **2023**, *145*, 1301–1309.
63. Yue, B.; Zhong, W.; Yu, X.; Hong, F. Superconductivity in the Van Der Waals Crystal SnS_2 Up to 105 GPa. *Phys. Rev. B* **2022**, *105*, 104514.
64. Zhang, H.; Zhong, W.; Meng, Y.; Tang, B.; Yue, B.; Yu, X.; Hong, F. Helicity Transitions and Emerging Superconductivity in Chiral α-HgS. *Phys. Rev. B* **2024**, *110*, L060502.
65. Zhong, W.; Zhang, H.; Karaca, E.; Zhou, J.; Kawaguchi, S.; Kadobayashi, H.; Yu, X.; Errandonea, D.; Yue, B.; Hong, F. Pressure-Sensitive Multiple Superconducting Phases and Their Structural Origin in Van Der Waals HfS_2 Up to 160 GPa. *Phys. Rev. Lett.* **2024**, *133*, 066001.
66. Liu, R.; Si, L.; Niu, W.; Zhang, X.; Chen, Z.; Zhu, C.; Zhuang, W.; Chen, Y.; Zhou, L.; Zhang, C.; Wang, P.; Song, F.; Tang, L.; Xu, Y.; Zhong, Z.; Zhang, R.; Wang, X. Light-Induced Mott Insulator-to-Metal Phase Transition in Ultrathin Intermediate-Spin Ferromagnetic Perovskite Ruthenates. *Adv. Mater.* **2023**, *35*, 2211612.
67. Li, C.; Wang, Y.; Liu, K.; Jiang, D.; Feng, J.; Wen, T.; Yue, B.; Zhou, Y.; Sun, L.; Wang, Y. Superconductivity in Quasi-One-Dimensional Ferromagnet $CrSbSe_3$ Under High Pressure. *J. Am. Chem. Soc.* **2024**, *146*, 9688–9696.
68. Stahl, Q.; Ritschel, T.; Garbarino, G.; Cova, F.; Isaeva, A.; Doert, T.; Geck, J. Pressure-Tuning of α-$RuCl_3$ Towards a Quantum Spin Liquid. *Nat. Commun.* **2024**, *15*, 8142.
69. Imai, Y.; Nawa, K.; Shimizu, Y.; Yamada, W.; Fujihara, H.; Aoyama, T.; Takahashi, R.; Okuyama, D.; Ohashi, T.; Hagihala, M.; Torii, S.; Morikawa, D.; Terauchi, M.; Kawamata, T.; Kato, M.; Gotou, H.; Itoh, M.; Sato, T. J.; Ohgushi, K. Zigzag Magnetic Order in the Kitaev Spin-Liquid Candidate Material $RuBr_3$ with a Honeycomb Lattice. *Phys. Rev. B* **2022**, *105*, L041112.
70. Ni, D.; Gui, X.; Powderly, K. M.; Cava, R. J. Honeycomb-Structure RuI_3, a New Quantum Material Related to α-$RuCl_3$. *Adv. Mater.* **2022**, *34*, 2106831.
71. Sun, Z.; Song, H.; Zhao, M. H.; Zeng, Y.; Li, M. R. Structural Determination and Exotic Resistive Behaviour of α-RuI_3 Under High-Pressure. *Chin. J. Struct. Chem.* **2025**, *44*, 100429.
72. Zhang, Y.; Lin, L. F.; Moreo, A.; Dagotto, E. Theoretical Study of the Crystal and Electronic Properties of α-RuI_3. *Phys. Rev. B* **2022**, *105*, 085107.
73. Jiang, D.; Jiang, X.; Zhang, X.; Li, C.; Liu, K.; Ma, Y.; Cheng, H. M.; Pei, T.; Wen, T.; Lin, Z.; Li, F.; Wang, Y. Second-Harmonic-Generation Switching via Pressure-Suppressed Dynamical Disorder. *J. Am. Chem. Soc.* **2024**, *146*, 23508–23516.
74. Li, Q.; Xu, B.; Quan, Z. Pressure-Regulated Excitonic Transitions in Emergent Metal Halides. *Acc. Chem. Res.* **2023**, *56*, 3282–3291.
75. Eremets, M. I.; Gavriliuk, A. G.; Trojan, I. A.; Dzivenko, D. A.; Boehler, R. Single-Bonded Cubic Form of Nitrogen. *Nat. Mater.* **2004**, *3*, 558–563.
76. Bykov, M.; Chariton, S.; Fei, H.; Fedotenko, T.; Aprilis, G.; Ponomareva, A. V.; Tasnadi, F.; Abrikosov, I. A.; Merle, B.; Feldner, P.; Vogel, S.; Schnick, W.; Prakapenka, V. B.; Greenberg, E.; Hanfland, M.; Pakhomova, A.; Liermann, H. P.; Katsura, T.; Dubrovinskaia, N.; Dubrovinsky, L. High-Pressure Synthesis of Ultraincompressible Hard Rhenium Nitride Pernitride $Re_2N_{(2)}(N)_2$ Stable at Ambient Conditions. *Nat. Commun.* **2019**, *10*, 2994.
77. Zhou, X.; Liang, Y.; Gu, C.; Fang, L.; Chen, B.; Zhao, Y.; Wang, S. Synthesis, Crystal Structure, Stability, and Mechanical Properties of the Hexagonal Tungsten Nitride $WN_{1-\delta}$. *Chem. Mater.* **2024**, *36*, 8514–8522.
78. Kawamura, F.; Imura, M.; Murata, H.; Yamada, N.; Taniguchi, T. Synthesis of a Novel Rocksalt-Type Ternary Nitride Semiconductor $MgSnN_2$ Using the Metathesis Reaction Under High Pressure. *Eur. J. Inorg. Chem.* **2019**, *2020*, 446–451.
79. Weidemann, M.; Werhahn, D.; Mayer, C.; Kläger, S.; Ritter, C.; Manuel, P.; Attfield, J. P.; Kloß, S. D. High-Pressure Synthesis of Ruddlesden–Popper Nitrides. *Nat. Chem.* **2024**, *16*, 1723–1731.
80. Wang, P.; Wang, Y.; Wang, L.; Zhang, X.; Yu, X.; Zhu, J.; Wang, S.; Qin, J.; Leinenweber, K.; Chen, H.; He, D.; Zhao, Y. Elastic, Magnetic and Electronic Properties of Iridium Phosphide Ir_2P. *Sci. Rep.* **2016**, *6*, 21787.
81. Song, J.; Fei, G.; Liu, X.; Duan, S.; Yang, B.; Chen, X.; Singh, D. J.; Liu, Y.; Yang, L.; Guo, J.; Zhang, P. Pressure-Driven Significant Phonon Mode Softening and Robust Superconductivity in Layered Germanium Phosphide. *J. Mater. Chem. A* **2020**, *8*, 20054–20061.
82. Ma, S.; Bao, K.; Tao, Q.; Zhu, P.; Ma, T.; Liu, B.; Liu, Y.; Cui, T. Manganese Mono-Boride, an Inexpensive Room Temperature Ferromagnetic Hard Material. *Sci. Rep.* **2017**, *7*, 43759.
83. Pei, C.; Zhang, J.; Wang, Q.; Zhao, Y.; Gao, L.; Gong, C.; Tian, S.; Luo, R.; Li, M.; Yang, W.; Lu, Z. Y.; Lei, H.; Liu, K.; Qi, Y. Pressure-Induced Superconductivity at 32 K in MoB_2. *Natl. Sci. Rev.* **2023**, *10*, nwad034.
84. Drozdov, A. P.; Eremets, M. I.; Troyan, I. A.; Ksenofontov, V.; Shylin, S. I. Conventional Superconductivity at 203 Kelvin at High Pressures in the Sulfur Hydride System. *Nature* **2015**, *525*, 73–76.
85. Liu, C.; Jiang, S.; Sui, Y.; Chen, Y.; Xiao, G.; Chen, X.-J.; Shu, H.; Duan, D.; Li, X.; Liu, H.; Zou, B. Effect of the Inherent Structure of Rh Nanocrystals on the Hydriding Behavior Under Pressure. *J. Phys. Chem. Lett.* **2019**, *10*, 774–779.
86. Shi, K.; Huo, Z.; Liang, T.; Sui, Y.; Liu, C.; Shu, H.; Wang, L.; Duan, D.; Zou, B. Harvesting Pdh Employing Pd Nano Icosahedrons via High Pressure. *Adv. Sci.* **2023**, *10*, 2205133.
87. Sheng, L.; Qi, G.; Jin, K.; Chen, A.; Huang, X.; Liu, G.; Zhou, M.; Wang, H.; Li, Y.; Wang, K.; Sui, Y.; Zou, B. Pressure Strategy to Improve H Atomic Utilization Via Optimized Decomposition Pathway in Solid Hydrazine Borane. *J. Phys. Chem. Lett.* **2024**, *15*, 9939–9944.
88. Ma, L.; Wang, K.; Xie, Y.; Yang, X.; Wang, Y.; Zhou, M.; Liu, H.; Yu, X.; Zhao, Y.; Wang, H.; Liu, G.; Ma, Y. High-Temperature Superconducting Phase in Clathrate Calcium Hydride CaH_6 Up to 215 K at a Pressure of 172 GPa. *Phys. Rev. Lett.* **2022**, *128*, 167001.
89. Wang, H.; Tse, J. S.; Tanaka, K.; Iitaka, T.; Ma, Y. Superconductive Sodalite-Like Clathrate Calcium Hydride at High Pressures. *Proc. Natl. Acad. Sci. U.S.A.* **2012**, *109*, 6463–6466.

DOI: 10.31635/ccschem.024.202405293
Citation: *CCS Chem.* **2025**, 7, 1250–1271
Link to VoR: https://doi.org/10.31635/ccschem.024.202405293

90. Peng, F.; Sun, Y.; Pickard, C. J.; Needs, R. J.; Wu, Q.; Ma, Y. Hydrogen Clathrate Structures in Rare Earth Hydrides at High Pressures: Possible Route to Room-Temperature Superconductivity. *Phys. Rev. Lett.* **2017**, *119*, 107001.
91. Drozdov, A. P.; Kong, P. P.; Minkov, V. S.; Besedin, S. P.; Kuzovnikov, M. A.; Mozaffari, S.; Balicas, L.; Balakirev, F. F.; Graf, D. E.; Prakapenka, V. B.; Greenberg, E.; Knyazev, D. A.; Tkacz, M.; Eremets, M. I. Superconductivity at 250 K in Lanthanum Hydride Under High Pressures. *Nature* **2019**, *569*, 528–531.
92. Liu, H.; Naumov, I. I.; Hoffmann, R.; Ashcroft, N. W.; Hemley, R. J. Potential High-T_c Superconducting Lanthanum and Yttrium Hydrides at High Pressure. *Proc. Natl. Acad. Sci. U.S.A.* **2017**, *114*, 6990–6995.
93. Feng, Y. J.; Jiang, M. J.; Ding, H. B.; Tian, H. L.; Lu, Z. H.; Zhong, G. H.; Yang, C. L.; Chen, X. J.; Lin, H. Q. High-Temperature Superconductivity in H_3S up to 253 K at a Pressure of 140 Gpa by Doping Holes. *J. Phys. Chem. C* **2022**, *126*, 20702–20709.
94. Zhou, X.; Zhao, M. H.; Yao, S. M.; Dong, H.; Wang, Y.; Chen, B.; Xing, X.; Li, M. R. Calibration of Local Chemical Pressure by Optical Probe. *Natl. Sci. Rev.* **2023**, *10*, nwad190.
95. Murnaghan, F. D. The Compressibility of Media Under Extreme Pressures. *Proc. Natl. Acad. Sci. U.S.A.* **1944**, *30*, 244–247.
96. Zhao, M. H.; Zhu, C.; Sun, Z.; Xia, T.; Han, Y.; Zeng, Y.; Gao, Z.; Gong, Y.; Wang, X.; Hong, J.; Zhang, W. X.; Wang, Y.; Yao, D. X.; Li, M. R. Methodological Approach to the High-Pressure Synthesis of Nonmagnetic $Li_2B^{4+}B'^{6+}O_6$ Oxides. *Chem. Mater.* **2022**, *34*, 186–196.
97. Han, Y.; Wu, M.; Gui, C.; Zhu, C.; Sun, Z.; Zhao, M. H.; Savina, A. A.; Abakumov, A. M.; Wang, B.; Huang, F.; He, L.; Chen, J.; Huang, Q.; Croft, M.; Ehrlich, S.; Khalid, S.; Deng, Z.; Jin, C.; Grams, C. P.; Hemberger, J.; Wang, X.; Hong, J.; Adem, U.; Ye, M.; Dong, S.; Li, M. R. Data-Driven Computational Prediction and Experimental Realization of Exotic Perovskite-Related Polar Magnets. *NPJ Quantum Mater.* **2020**, *5*, 92.
98. Sun, Z.; Yang, J.; Han, Y.; Li, M. R. Data-Driven High-Throughput Screening and Experimental Realization of $Ag_2B(IV)B'(VI)O_6$ Under Negative Chemical-Pressure. *Chem. Mater.* **2024**, *36*, 6740–6747.
99. Ma, Z.; Liu, Z.; Lu, S.; Wang, L.; Feng, X.; Yang, D.; Wang, K.; Xiao, G.; Zhang, L.; Redfern, S. A. T.; Zou, B. Pressure-Induced Emission of Cesium Lead Halide Perovskite Nanocrystals. *Nat. Commun.* **2018**, *9*, 4506.
100. Shi, Y.; Ma, Z.; Zhao, D.; Chen, Y.; Cao, Y.; Wang, K.; Xiao, G.; Zou, B. Pressure-Induced Emission (PIE) of One-Dimensional Organic Tin Bromide Perovskites. *J. Am. Chem. Soc.* **2019**, *141*, 6504–6508.
101. Shi, Y.; Zhao, W.; Ma, Z.; Xiao, G.; Zou, B. Self-Trapped Exciton Emission and Piezochromism in Conventional 3D Lead Bromide Perovskite Nanocrystals Under High Pressure. *Chem. Sci.* **2021**, *12*, 14711–14717.
102. Geng, T.; Shi, Y.; Liu, Z.; Zhao, D.; Ma, Z.; Wang, K.; Dong, Q.; Xiao, G.; Zou, B. Pressure-Induced Emission from All-Inorganic Two-Dimensional Vacancy-Ordered Lead-Free Metal Halide Perovskite Nanocrystals. *J. Phys. Chem. Lett.* **2022**, *13*, 11837–11843.
103. Zhao, W.; Ma, Z.; Shi, Y.; Fu, R.; Wang, K.; Sui, Y.; Xiao, G.; Zou, B. Pressure Tailoring Electron-Phonon Coupling Toward Enhanced Yellow Photoluminescence Quantum Yield and Piezochromism. *Cell Rep. Phys. Sci.* **2023**, *4*, 101663.
104. Zhao, W.; Fu, R.; Yang, J.; Xiao, G.; Zou, B. Building New Structural Distortion Descriptors Through Pressure Engineering Toward Enhanced Violet Emission in 2D Hybrid Perovskite. *Adv. Opt. Mater.* **2024**, *12*, 2401732.
105. Zhao, D.; Wang, M.; Xiao, G.; Zou, B. Thinking About the Development of High-Pressure Experimental Chemistry. *J. Phys. Chem. Lett.* **2020**, *11*, 7297–7306.
106. Ma, Z.; Yang, S.; Shi, Y.; Fu, Y.; Wang, K.; Xiao, G.; Zou, B. Considerable Piezochromism in All-Inorganic Zero-Dimensional Perovskite Nanocrystals via Pressure-Modulated Self-Trapped Exciton Emission. *Angew. Chem. Int. Ed.* **2024**, *63*, e202406015.
107. Xiao, Z.; Shan, S.; Wang, Y.; Zheng, H.; Li, K.; Yang, X.; Zou, B. Harvesting Multicolor Photoluminescence in Nonaromatic Interpenetrated Metal-Organic Framework Nanocrystals via Pressure-Modulated Carbonyls Aggregation. *Adv. Mater.* **2024**, *36*, 2403281.
108. Pan, D.; An, L.; Sun, Z.; Hou, W.; Yang, Y.; Yang, Z.; Lu, Y. Synthesis of Cu-In-S Ternary Nanocrystals with Tunable Structure and Composition. *J. Am. Chem. Soc.* **2008**, *130*, 5620–5621.
109. Kruszynska, M.; Borchert, H.; Parisi, J.; Kolny-Olesiak, J. Synthesis and Shape Control of $CuInS_2$ Nanoparticles. *J. Am. Chem. Soc.* **2010**, *132*, 15976–15986.
110. Xiao, N.; Zhu, L.; Wang, K.; Dai, Q.; Wang, Y.; Li, S.; Sui, Y.; Ma, Y.; Liu, J.; Liu, B.; Zou, G.; Zou, B. Synthesis and High-Pressure Transformation of Metastable Wurtzite-Structured $CuGaS_2$ Nanocrystals. *Nanoscale* **2012**, *4*, 7443.
111. Xiao, G.; Yang, X.; Zhang, X.; Wang, K.; Huang, X.; Ding, Z.; Ma, Y.; Zou, G.; Zou, B. A Protocol to Fabricate Nanostructured New Phase: B31-Type MnS Synthesized Under High Pressure. *J. Am. Chem. Soc.* **2015**, *137*, 10297–10303.
112. Wang, Y.; Liu, H.; Wu, M.; Wang, K.; Sui, Y.; Liu, Z.; Lu, S.; Nie, Z.; Tse, J. S.; Yang, X.; Zou, B. New-Phase Retention in Colloidal Core/Shell Nanocrystals via Pressure-Modulated Phase Engineering. *Chem. Sci.* **2021**, *12*, 6580–6587.
113. Lv, P.; Ma, Z.; Ning, J.; Xiao, G.; Zou, B. Identification of Defect Origin and White-Light Emission Tuning of Chalcogenide Quantum Dots Through Pressure Engineering. *CCS Chem.* **2025**, *7*, 160–169.
114. Cong, M.; Zhao, D.; Yang, J.; Xiao, G.; Zou, B. Identifying Organic-Inorganic Interaction Sites Toward Emission Enhancement in Non-Hydrogen-Bonded Hybrid Perovskite via Pressure Engineering. *Research* **2024**, *7*, 0476.
115. Fang, Y.; Zhang, L.; Yu, Y.; Yang, X.; Wang, K.; Zou, B. Manipulating Emission Enhancement and Piezochromism in Two-Dimensional Organic-Inorganic Halide Perovskite $[(HO)(CH_2)_2NH_3)]_2PbI_4$ by High Pressure. *CCS Chem.* **2020**, *3*, 2203–2210.
116. Ma, Z.; Li, F.; Zhao, D.; Xiao, G.; Zou, B. Whether or Not Emission of Cs_4PbBr_6 Nanocrystals: High-Pressure Experimental Evidence. *CCS Chem.* **2020**, *2*, 71–80.

DOI: 10.31635/ccschem.024.202405293
Citation: *CCS Chem.* **2025**, 7, 1250–1271
Link to VoR: https://doi.org/10.31635/ccschem.024.202405293

117. Ma, Z.; Xiao, G.; Zou, B. Step Forward to Light Up the Future: Pressure-Induced Emission. *Sci. Bull.* **2023**, *68*, 1588–1590.
118. Li, S.; Li, Q.; Wang, K.; Zhou, M.; Huang, X.; Liu, J.; Yang, K.; Liu, B.; Cui, T.; Zou, G.; Zou, B. Pressure-Induced Irreversible Phase Transition in the Energetic Material Urea Nitrate: Combined Raman Scattering and X-Ray Diffraction Study. *J. Phys Chem. C* **2012**, *117*, 152–159.
119. Li, S.; Li, Q.; Li, R.; Liu, J.; Yang, K.; Liu, B.; Zou, B. New Assembly of Acetamidinium Nitrate Modulated by High Pressure. *J. Phys Chem. C* **2014**, *118*, 23443–23450.
120. Fu, R.; Zhao, W.; Wang, L.; Ma, Z.; Xiao, G.; Zou, B. Pressure-Induced Emission Toward Harvesting Cold White Light from Warm White Light. *Angew. Chem. Int. Ed.* **2021**, *60*, 10082–10088.
121. Zhao, D.; Xiao, G.; Liu, Z.; Sui, L.; Yuan, K.; Ma, Z.; Zou, B. Harvesting Cool Daylight in Hybrid Organic-Inorganic Halides Microtubules Through the Reservation of Pressure-Induced Emission. *Adv. Mater.* **2021**, *33*, e2100323.
122. Zhao, D.; Cong, M.; Liu, Z.; Ma, Z.; Wang, K.; Xiao, G.; Zou, B. Steric Hindrance Effects on the Retention of Pressure-Induced Emission toward Scintillators. *Cell Rep. Phys. Sci.* **2023**, *4*, 101445.
123. Wang, Y.; Yang, X.; Liu, C.; Liu, Z.; Fang, Q.; Bai, F.; Wang, S.; Hou, X.; Feng, B.; Chen, B.; Zou, B. Maximized Green Photoluminescence in Tb-Based Metal-Organic Framework via Pressure-Treated Engineering. *Angew. Chem. Int. Ed.* **2022**, *61*, e202210836.
124. Wang, Y.; Liu, C.; Yong, X.; Yang, X.; Yu, J.; Lu, S.; Bai, F.; Wang, S.; Wang, K.; Liu, Z.; Feng, B.; Hou, X.; Liu, H.; Chen, B.; Fang, Q.; Zou, B. Pressure Engineering Toward Harvesting the Bright Deep-Blue-Light Emission in Y-Based Metal-Organic Frameworks. *Adv. Funct. Mater.* **2023**, *33*, 2300109.
125. Zhang, T.; Yong, X.; Yu, J.; Wang, Y.; Wu, M.; Yang, Q.; Hou, X.; Liu, Z.; Wang, K.; Yang, X.; Lu, S.; Zou, B.. Brightening Blue Photoluminescence in Nonemission MOF-2 by Pressure Treatment Engineering. *Adv. Mater.* **2023**, *35*, e2211729.
126. Yang, Q.; Yang, X.; Wang, Y.; Fei, Y.; Li, F.; Zheng, H.; Li, K.; Han, Y.; Hattori, T.; Zhu, P.; Zhao, S.; Fang, L.; Hou, X.; Liu, Z.; Yang, B.; Zou, B. Brightening Triplet Excitons Enable High-Performance White-Light Emission in Organic Small Molecules via Integrating n-π^*/π-π^* Transitions. *Nat. Commun.* **2024**, *15*, 7778.

DOI: 10.31635/ccschem.024.202405293
Citation: *CCS Chem.* **2025**, 7, 1250–1271
Link to VoR: https://doi.org/10.31635/ccschem.024.202405293